JOURNAL OF PETROLOGY | VOLUME 51 | NUMBER 6 | PAGES 1237–1266 | 2010 | doi:10.1093/petrology/egq017

Continent Formation in the Archean and Chemical Evolution of the Cratonic Lithosphere: Melt–Rock Reaction Experiments at 3–4 GPa and Petrogenesis of Archean Mg-Diorites (Sanukitoids)

R. P. RAPP[1,2,3]*, M. D. NORMAN[1], D. LAPORTE[3,4], G. M. YAXLEY[1], H. MARTIN[3,4] AND S. F. FOLEY[5]

[1]RESEARCH SCHOOL OF EARTH SCIENCES, AUSTRALIAN NATIONAL UNIVERSITY, CANBERRA, ACT 0200, AUSTRALIA

[2]MINERAL PHYSICS INSTITUTE, DEPARTMENT OF GEOSCIENCES, STONY BROOK UNIVERSITY, STONY BROOK, NY 11794-2100, USA

[3]CLERMONT UNIVERSITÉ, UNIVERSITÉ BLAISE PASCAL, LABORATOIRE MAGMAS ET VOLCANS, BP 10448, F-63000 CLERMONT-FERRAND, FRANCE

[4]CNRS, UMR 6524, LMV, F-63038 CLERMONT-FERRAND, FRANCE

[5]IRD, R 163, LMV, F-63038 CLERMONT-FERRAND, FRANCE

RECEIVED AUGUST 20, 2009; ACCEPTED MARCH 23, 2010

To better understand the genetic relationship between granitoid rocks of the Archean cratons and the underlying 'keel' of subcratonic lithospheric mantle (SCLM), we have conducted two types of experiments in a multi-anvil apparatus at 3–4 GPa: (1) peridotite assimilation experiments, in which natural, hydrous TTG (trondhjemite–tonalite–granodiorite) melts are reacted with mantle peridotite at relatively high melt–rock ratios; (2) liquidus saturation experiments on hydrous Mg-rich diorite (sanukitoid) melts. Our results demonstrate that liquids similar to typically late- to post-tectonic sanukitoid intrusions can form by hybridization of initial TTG melts by assimilation of olivine-bearing peridotite, and that these primitive granitoid melts are in equilibrium with reaction residues consisting of olivine-free garnet websterite or garnet pyroxenite. The experimental melts retain the distinctive trace element signature of TTGs, overprinted by a 'primitive' mantle signature (i.e. high Mg-number, elevated Cr and Ni abundances), whereas the various phases of the crystalline residues acquire trace element signatures reflecting equilibration with Mg-rich granitoid melts. At low melt:rock ratios, metasomatism by TTG melts may be responsible for the silica enrichment and high modal orthopyroxene content of some cratonic peridotites and cryptic trace element overprints in garnet, clinopyroxene, and orthopyroxene. Our results demonstrate that the lithospheric keel of Archean cratons represents the product of reaction between TTG melts and previously depleted mantle peridotite at relatively low melt:rock ratios, as evidenced by the trace element signature in garnet pyroxenite and orthopyroxene-enriched garnet peridotite xenoliths, whereas Late Archean sanukitoids represent the products of these same reactions at relatively high melt:rock ratios.

KEY WORDS: *TTG; cratons; cratonic lithosphere; garnet websterite; sanukitoid*

INTRODUCTION

Despite indirect evidence for the presence of continental crust on the Earth at ~4·2–4·4 Ga (Harrison *et al.*, 2005;

*Corresponding author. Present address: Research School of Earth Sciences, Australian National University, Canberra, ACT 0200, Australia. Tel.: 61-02-6125-7671. Fax: 61-02-6125-8253. E-mail: robert.rapp@anu.edu.au

Harrison, 2009), no granitoid rocks older than ~4·0 Ga survive and so the question of when and how Earth's first true continents formed remains a matter for continued speculation and debate. Archean cratons, the nuclei for the continents, have been attached to deep roots or 'keels' in the cratonic lithosphere since their initial formation more than 3·0 Ga ago (Carlson *et al.*, 2000, 2005; James & Fouch, 2002; Pearson *et al.*, 2002; Lee & Aeolus, 2006; Arndt *et al.*, 2009). The physical and temporal juxtaposition of the oldest preserved granitoid rocks with old, cold roots extending deep into the underlying subcratonic lithospheric mantle (SCLM) implies a coeval evolutionary history; preservation of this oldest continental crust may in fact be contingent upon the development of these deep roots in the cratonic lithosphere. Understanding the genetic relationship between Archean continental crust and the SCLM may therefore be crucial to understanding how physically and chemically stable continental nuclei (cratons) formed on Earth.

The vast majority of continental crust of early to mid-Archean age (~3·8–3·0 Ga) is composed of granitoids of the TTG (trondhjemite–tonalite–granodiorite) suite of plutonic rocks (Martin *et al.*, 2005). A survey of all Archean granitoids in terms of a simple geochemical parameter, the Mg-number (defined as the molar ratio of [Mg/(Mg + Fe)], which in the present context reflects the extent of direct mantle contributions to granitoid petrogenesis), shows that Archean granitoids with Mg-numbers greater than ~0·50 are relatively rare in the rock record prior to ~3·5 Ga, but become increasingly more common between 3·5 and 3·0 Ga (Fig. 1). By 3·0 Ga, late- to post-tectonic granitoids of the sanukitoid suite (Shirey & Hanson, 1984; Stern & Hanson, 1991), with Mg-numbers of ~0·55 and above, have become prevalent (Fig. 1), although granitoids of the TTG suite, with Mg-numbers less than 0·50, still predominate crust-generating processes throughout this period. Although granitoids of the TTG suite occur predominantly in the Archean, intrusive rocks of comparable composition are also found in much younger terranes (e.g. in the northern and central Andes; Petford & Atherton, 1996; Bourdon *et al.*, 2002; Condie, 2005; Figueroa *et al.*, 2009), and compositionally similar intrusive and extrusive rocks occur throughout the geological record, from the Archean to the present, and are often referred to as 'adakites'. The similarities and differences between adakites and TTG have been discussed in detail in a number of recent papers (e.g. Smithies, 2000; Condie, 2005; Martin *et al.*, 2005, 2010), and as their relationship continues to be a matter of considerable debate, this is a subject beyond the scope of this paper. Suffice it to say that, despite their overall similarities in terms of major- and trace-element characteristics, there is general agreement that adakites have higher Mg-numbers than TTGs, with a consensus that TTGs are restricted to Na-rich granitoids with Mg-numbers less than ~0·50.

A number of experimental studies have shown that the chemical compositions of TTG granitoids are consistent with an origin by low to moderate degrees of dehydration melting of garnet-bearing metabasalt (garnet amphibolite

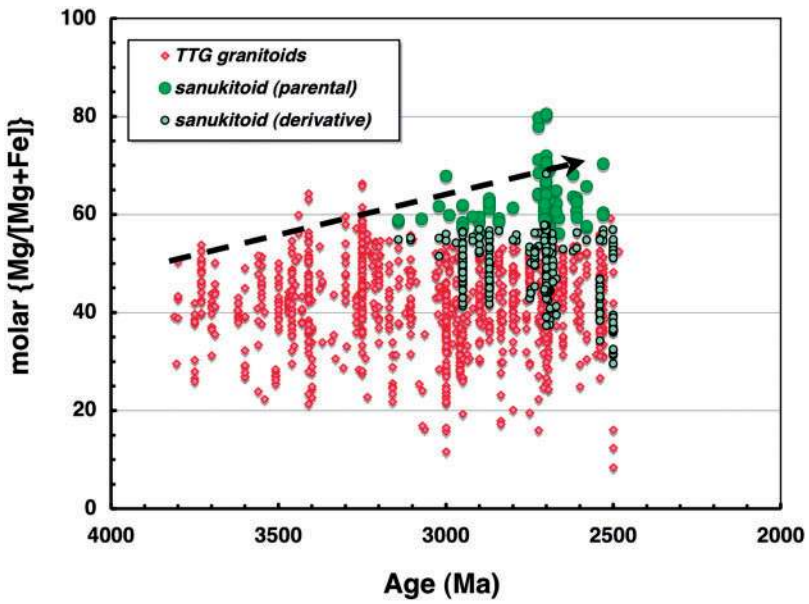

Fig. 1. Mg-number vs age for Archean granitoids, including tonalite–trondhjemite–granodiorites (TTG), 'parental' sanukitoids with Mg-numbers >0·58, and 'derivative' sanukitoid suite granitoids formed by crystallization differentiation of 'parental' sanukitoids. Sanukitoids are distinguished from TTGs on the basis of their Mg-number and K_2O/Na_2O ratio (>1·0 for sanukitoids; ≪1·0 for TTG). It should be noted that TTG production does not cease in the Archean, but continues up to the present day in some locales.

to eclogite; e.g. Rapp *et al.*, 1991, 2003; Sen & Dunn, 1994*a*; Rapp & Watson, 1995). The relative scarcity of early to mid-Archean granitoids with 'primitive' geochemical characteristics, indicative of a mantle petrogenetic lineage, suggests that there was limited mantle participation in granitoid magmatism prior to 3·0 Ga. It is only with the appearance in the Late Archean of monzodiorites and trachyandesites of the sanukitoid suite that granitoids with a direct mantle pedigree are found in any significant quantities (it should be noted that although most early to mid-Archean TTG have $+\varepsilon_{Nd}$, this mantle isotopic signature is probably acquired indirectly through remelting of basaltic precursors), with the implication that these magmas mark the maturation of crustal growth processes and the beginning of 'modern-style' subduction-related arc magmatism in a plate-tectonic framework [e.g. downgoing slab, overlying mantle wedge, and crustal growth via some variant of 'the andesite model' (Arculus, 2006); see also Smithies (2000), Smithies & Champion (2000), Martin & Moyen (2002) and Martin *et al.* (2005, 2010) for discussion of the evolution in tectonic style through the Archean, and Bedard (2006) for an alternative, plume-based model].

The compositional transition in granitoid magmatism *c.* 3·0 Ga represents the establishment of a clear genetic link between rocks of the silica-rich continental crust and ultramafic rocks of the subcontinental lithospheric mantle. In this study, this relationship is considered from two perspectives: first, the nature of the reaction between TTG liquids and peridotitic (cratonic) mantle and its effect on the composition of the hybridized melt; second, the role of TTG melts as metasomatic agents within the cratonic lithosphere. Our focus is on reactions between TTG–sanukitoid melts and mantle peridotite in the juvenile root zones of a maturing Archean craton.

EXPERIMENTAL AND ANALYTICAL METHODS

Natural starting materials were selected for the laboratory experiments described below. Where published data were not available, bulk compositions were determined for major elements by X-ray fluorescence (XRF) in Clermont-Ferrand and solution inductively coupled plasma mass spectrometry (ICP-MS) for trace elements at the Australian National University (ANU) (Table 1). The granitoid rocks used in the experiments include a primitive tonalitic 'old grey gneiss' (Table 1, SV-4: Mg-number = 0·36; $K_2O/Na_2O = 0{\cdot}33$) from the 3·4 Ga Sete Voltas massif in the Brazilian Craton (Martin *et al.*, 1997), and two primitive, Late Archean sanukitoid compositions from the granite–greenstone terranes of the Superior Province: the 2·7 Ga old Saganaga Tonalite (ST-01: Mg-number = 0·54; $K_2O/Na_2O = 0{\cdot}33$) from the Minnesota River Valley, provided by G. Hanson of Stony Brook University (Arth & Hanson, 1972; Goldich *et al.*, 1972), and a 2·7 Ga monzodiorite (RR-07: Mg-number = 0·61; $K_2O/Na_2O = 0{\cdot}52$) from the Roaring River Complex (Stern & Hanson, 1991). The latter two samples possess the elevated Mg-numbers and Cr and Ni contents characteristic of the Late Archean Mg-rich diorites and monzodiorites that were initially described by Shirey & Hanson (1984), and first given the name 'sanukitoid', whereas the Sete Voltas tonalite has a low Mg-number typical of the early to mid-Archean TTG suite; all three granitoids have the high Sr/Y and La/Yb ratios and low Y and Yb concentrations characteristic of Archean TTGs and sanukitoids. A hydrous glass of SV-4 with *c.* 6 wt % H_2O was synthesized in an internally heated pressure vessel at 0·25 GPa and 900°C at the Laboratoire Magmas et Volcans, Blaise Pascal University in Clermont-Ferrand; in experiments with the sanukitoid starting materials (ST-01 and RR-07 monzodiorites), *c.* 6–8 wt % H_2O was added to the charge by microsyringe. The peridotite samples consist of rock powders made directly from two different depleted spinel peridotite xenoliths derived from the sub-arc mantle beneath the northern sector of the Kamchatka Arc (Kepezhinskas *et al.*, 1995, 1996) (Table 1). These peridotites were selected on the basis of their depleted nature, the fact that they had been previously described, and because they could be compared with other xenoliths from the same xenolith collection that had undergone variable degrees of adakite metasomatism (Kepezhinskas *et al.*, 1995, 1996). In addition, a single garnet peridotite xenolith from the Matsoku kimberlite in Lesotho, collected during the 7th International Kimberlite Conference field trip in 1998, was analyzed for major and trace elements for comparison with the experimental run products.

Two types of experiments were carried out: (1) liquidus saturation experiments on the RR-07 sanukitoid composition; (2) peridotite assimilation experiments, in which either the SV-4 tonalite glass or the ST-01 rock powder was mixed in fixed proportions with powdered peridotite DP-1 or DP-2. With one exception, all of the experiments were conducted in a Walker-type multi-anvil apparatus at Stony Brook University at pressures of 3·5–3·8 GPa and temperatures of 1100–1250°C, using thick-walled (~1 mm), pressure welded, Au_{100} capsules. One additional peridotite assimilation experiment using the hydrated SV-4 glass was carried out at 3·0 GPa and 1100°C in a piston-cylinder apparatus at the Laboratoire Magmas et Volcans in Clermont-Ferrand, using instead a thick-walled Au_{80}–Pd_{20} capsule. The experiments were maintained at the high P–T conditions for 5–10 days; after quenching, the sample capsules were sectioned and polished for microanalysis. A summary of run conditions and the resulting high-pressure phase assemblages is provided in Table 2.

Table 1: Whole rock major- and trace-element compositions of experimental starting materials (Columns 1–5), and of a garnet websterite xenolith from the Matsoku kimberlite, Lesotho (Column 6)

Sample:	1	2	3	4	5	6
Label:	SV4	ST-01	RR-07	DP1	DP2	MAT-1
Type:	TTG	Mg-diorite	sanukitoid	peridotite	peridotite	xenolith
wt % oxide						
SiO_2	66·44	62·98	58·81	44·48	42·27	46·60
TiO_2	0·50	0·29	0·49	0·0	0·17	0·03
Al_2O_3	16·76	18·51	16·15	0·69	2·75	1·55
FeO	4·32	3·26	4·81	7·43	n.a	n.a.
Fe_2O_3	n.a.	n.a.		n.a.	11·44	6·48
MnO	0·09	0·08	0·09	0·12	0·16	0·10
MgO	1·39	2·76	4·30	43·85	38·54	42·19
CaO	4·13	4·18	6·31	0·91	2·97	0·79
Na_2O	5·15	5·43	5·22	0·31	0·11	0·11
K_2O	1·02	1·77	2·73	0·04	0·007	0·18
P_2O_5	0·20	0·08	0·48	n.d.	0·013	0·025
Cr_2O_3	b.d.	b.d.	n.a.	0·43	n.a.	0·261
H_2O_T	n.a.	n.a.	n.a.	0·0	2·29	0·00
Total	100·00	99·34	99·39	98·38	98·44	100·60
Mg-no.	0·37	0·54	0·61	0·86	0·87	0·93
Trace elements (ppm)						
Sc	n.a.	8·1	11	14·0	12·9	6·6
V	30·5	44	83	36	38	26·4
Co	8·05	12	20	127	111	90
Cr	18·0	106	143	2903	—	1786
Ni	15·8	39	80	2752	2113	19
Rb	68·6	54·1	26·2	0·04	0·089	7·86
Sr	571	698	1943	141	88	30.
Y	9·5	5·51	12·7	0·09	2·8	0·44
Zr	219	24·0	20·3	0·16	6·97	5·50
Nb	3·75	3·00	2·48	0·040	0·092	2·17
Cs	2·41	1·33	0·46	0·0012	0·004	0·24
Ba	188	673	2432	3·2	4·44	13·9
La	22·11	20·6	60·4	0·022	0·41	1·36
Ce	48·6	42·1	122·8	0·049	1·21	2·90
Nd	20·8	16·8	58·8	0·029	1·11	1·41
Sm	3·73	2·64	9·95	0·007	0·35	0·25
Eu	1·18	0·73	2·77	0·002	0·13	0·070
Gd	2·72	1·81	6·27	0·008	0·46	0·186
Dy	1·87	1·03	2·84	0·009	0·52	0·106
Er	0·79	0·51	1·04	0·011	0·29	0·037
Yb	0·67	0·51	0·75	0·024	0·28	0·031
Hf	4·59	0·076	0·110	0·004	0·20	0·104
Ta	0·19	0·19	0·095	0·004	0·011	0·110
Pb	17·9	7·9	15·9	0·25	0·71	0·1
Th	0·49	3·37	1·81	0·005	0·013	0·181
U	0·66	0·63	0·29	0·004	0·012	0·063

Whole-rock major elements by XRF and trace elements by solution ICP-MS for samples 1, 4, 5 and 6; published analyses for samples 2 and 3; n.a., not analyzed. Sample localities: (1) SV4 TTG: Sete Voltas TTG from the Brazilian Craton; (2) Saganaga Tonalite (ST-002): Mg-rich diorite from the Vermilion district granite–greenstone terrane, Minnesota River Valley, northeastern Minnesota–northwestern Ontario, provided by Professor G. Hanson, Stony Brook University, Stony Brook, NY, USA (after Goldich *et al.*, 1972); (3) Roaring River monzodiorite (MZDi-07): 'sanukitoid' from the Superior Province, Canada (Stern & Hanson, 1991); (4) depleted peridotite AVX-51 (DP1): ultradepleted harzburgite xenolith from Valvoyam Volcanic Field (VVF), northern Kamchatka (Kepezhinskas *et al.*, 1995); (5) melt-metasomatized, 'depleted' spinel peridotite xenolith 8710P (DP2): also from VVF, Kamchatka sub-arc mantle; (6) garnet pyroxenite xenolith from the Matsoku kimberlite, Lesotho (this study) MAT-1: modal composition: orthopyroxene 46·8%, garnet 6 ·2%, olivine 44·0%, clinopyroxene 3·0%, phlogopite, <1·0%; residual sums 0·99.

Table 2: Experimental run conditions and high-pressure phase assemblages

Run	Material	*P* (GPa)	*T* (°C)	Assemblage
KJ2	RR-07 + 6 wt % H_2O	3·8	1250	Cpx, melt
KJ3	RR-07 + 6 wt % H_2O	3·8	1220	gt, Cpx, melt
KJ4	RR-07 + 6 wt % H_2O	3·8	1200	gt, Cpx, melt
KJ6	RR-07 + 6 wt % H_2O + 33% DP1	3·8	1250	gt, Cpx, melt
ST/DP1	ST-01 + 30% DP1	3·6	1150	gt, Opx, Cpx, melt
ST/DP2	ST-01 + 30% DP1	3·8	1200	gt, Opx, Cpx, melt
ST/DP3	ST-01 + 50% DP1	3·8	1200	gt, Opx, melt
CF-HP	SV4 + 30% DP2	3·0	1100	gt, Cpx, Opx, phlg, melt

Starting materials: RR-07, Roaring River Sanukitoid (Stern & Hanson, 1991); DP1, depleted peridotite 'AVX51', from Valvoyam Volcanic Field, northern Kamchatka (Kepezhinskas *et al.*, 1995; bulk composition reported by Rapp *et al.*, 1999); ST-01, Saganaga Tonalite (Goldich *et al.*, 1972); SV4, 3·4 Ga old TTG from the Sete Voltas massif, Brazilian Craton (Martin *et al.*, 1997); DP2, depleted peridotite 8710P from Valvoyam Volcanic Field, northern Kamchatka (Kepezhinskas *et al.*, 1995).

The phase assemblages consisted of a glass (quenched melt) and coexisting metasomatic crystalline phases; no relicts of the original peridotite minerals were evident (e.g. unreacted cores). The glasses and crystals were characterized for major elements by electron microprobe analysis (EPMA; Cameca SX100 at ANU for major elements), and for trace elements by laser-ablation (Excimer UV) ICP-MS (HP7500 Agilent) at ANU. EPMA analyses were conducted with an accelerating voltage of 15 kV, a beam current of 20 nA and a focused beam (~1 μm diameter) for the crystalline phases, and a beam current of 10 nA and a defocused beam (~20 μm diameter) for analyses of the glasses (to minimize Na loss under the electron beam). For the laser-ablation ICP-MS analyses, the largest possible laser beam size was used to maximize signal intensity, with the size of the crystals and/or melt pockets being the limiting factor (generally a beam diameter of ≤30 μm was required). Glasses of NIST-612 and NIST-610 (Hinton, 2007), and USGS geochemical reference standard BCR-2 (Ila & Frey, 1999) and Geological Survey of Japan rock standard JA-1 (Ando *et al.*, 1987), were used as primary and secondary standards, respectively, with CaO wt % determined by EPMA used as an internal standard.

RESULTS

General observations

All of the experiments produced high Mg-number dioritic melts in equilibrium with garnet pyroxenite or garnet websterite crystalline reaction residues; none of the original peridotitic olivine of the starting materials survived the melt–rock reaction. Major-element compositions of the melts and minerals are given in Tables 2 and 3, respectively, and the trace element compositions of selected crystalline phases are given in Table 4 (for both melts and minerals). Modest thermal gradients (~20–30°C over ~1 mm) along the length of the sample capsules in the multi-anvil experiments produce layered textures, with a zone of crystal-free melt overlying layers of crystals with small amounts of interstitial melt, and with the liquidus phase closest to the top. These textures were advantageous in isolating a particular phase when aiming the laser beam for the ICP-MS analyses. Back-scattered electron photomicrographs of polished sections of several of the experimental charges are shown in Fig. 2a–d. The distribution of phases was much more uniform in the single piston-cylinder experiment (CF-HP; Fig. 2d).

In the sanukitoid liquidus saturation experiments with the RR-7 starting material, near-liquidus melts with moderate Mg-numbers (~0·46–0·53) coexist with garnet pyroxenite [e.g. clinopyroxene (Cpx) + subordinate garnet (gt)] or garnet websterite (gt + Cpx + Opx) crystalline reaction residues. For example, the phase assemblage in experiment KJ-2, which at ~1250°C is the highest temperature run and therefore closest to the liquidus at 3·8 GPa, consists of 72% melt, 22% clinopyroxene, and 6% garnet, by weight per cent mass-balance caculation (residue = 78% Cpx, 22% gt); experiments KJ-3 and KJ-4, at slightly lower temperatures (1200–1220°C), consist of 49–51% melt, ~42% clinopyroxene, and ~12% garnet (residue = 77% Cpx, 23% gt). These results suggest that hydrous sanukitoid liquids at 3·8 GPa (~140–150 km depth) would have been in equilibrium with a garnet clinopyroxenite phase assemblage, formed in response to reaction between hydrous TTG melts and fertile peridotite, with clinopyroxene the liquidus phase (see below). Experiment KJ-6, in which ~30% peridotite rock powder was added

Table 3: Major-element compositions of melts and crystalline phases in sanukitoid liquidus and TTG or sanukitoid melt–peridotite rock reaction experiments, and of phases in garnet peridotite xenolith from Matsoku kimberlite, Lesotho

Sample:	KJ-2	KJ-3	KJ-4	KJ-6	ST/DP_{30}1	ST/DP_{30}2	ST/DP 3	CF-HP
P (GPa):	3·8	3·8	3·8	3·8	3·5	3·5	3·8	3·0
T (°C):	1250	1220	1200	1250	1150	1200	1200	1100
wt % oxide								
SiO_2	54·38	59·34	61·51	56·67	67·34	63·13	55·71	58·24
TiO_2	0·58	0·72	0·95	0·54	0·42	0·66	0·33	0·69
Al_2O_3	14·02	12·80	12·78	12·09	9·87	15·31	12·49	15·20
FeO*	3·45	2·24	2·23	3·20	1·53	2·73	3·11	2·63
MnO	0·03	0·052	0·06	0·06	0·02	0·06	0·04	0·08
MgO	2·17	1·13	1·04	5·95	2·77	1·89	5·25	1·86
CaO	3·80	2·88	2·86	3·71	1·03	3·88	3·64	3·27
Na_2O	3·92	3·67	3·52	5·13	3·02	3·93	5·66	6·03
K_2O	3·33	5·64	6·26	3·09	4·41	3·30	2·61	2·18
P_2O_5	0·68	0·85	0·89	0·58	0·17	0·78	0·27	0·49
Cr_2O_3	n.d.	n.d.	b.d.	0·027	n.d.	b.d.	n.d.	0·01
Total	86·36	88·81	92·10	90·58	90·14	95·67	88·37	90·65
Mg-no.	0·53	0·48	0·46	0·77	0·76	0·55	0·77	0·56

Sample:	KJ-2	KJ-2	KJ-3	KJ-3	KJ-4	KJ-4	KJ-6	KJ-6
P (GPa):	3·8	3·8	3·8	3·8	3·8	3·8	3·8	3·8
T (°C):	1250	1250	1220	1220	1200	1200	1250	1250
Phase:	gt	Cpx	gt	Cpx	gt	Cpx	gt	Cpx
wt % oxide								
SiO_2	40·96(0·27)	53·90(0·16)	39·32	55·97	40·10	56·43	42·70(0·27)	56·26(0·77)
TiO_2	0·31(0·04)	0·13(0·03)	0·35	0·29	0·19	0·30	0·23(0·02)	0·13(0·01)
Al_2O_3	22·45(0·15)	14·08(0·39)	20·76	15·57	22·40	15·57	23·13(0·16)	8·91(0·29)
FeO*	11·29(0·07)	5·03(0·24)	19·22	3·29	16·80	3·70	7·90(0·39)	2·86(0·10)
MnO	0·49(0·04)	0·02(0·01)	0·46	0·06	0·36	0·15	0·22(0·03)	0·08(0·02)
MgO	14·25(0·37)	7·76(0·42)	9·21	6·59	11·54	6·75	22·00(0·32)	14·74(0·28)
CaO	8·95(0·21)	11·23(0·43)	8·56	9·79	8·14	10·16	3·49(0·21)	11·03(0·10)
Na_2O	0·12(0·02)	6·41(0·21)	0·21	7·43	0·23	7·26	0·14(0·03)	5·10(0·20)
K_2O	0·01(0·01)	0·02(0·01)	0·03	0·03	0·02	0·13	0·01(0·004)	0·01(0·01)
P_2O_5	0·22(0·03)	b.d.	0·36	0·07	0·33	b.d.	0·08(0·02)	0·02(0·01)
Cr_2O_3	n.a.	0·17(0·04)	0·16	0·004	0·01	0·06	0·27(0·05)	0·14(0·03)
Total	99·05	98·75	98·64	100·30	100·13	100·46	100·17	99·29
Mg-no.	0·69	0·73	0·46	0·78	0·55	0·77	0·84	0·90
		$Mg_{42}Fe_{15}Ca_{43}$	$Py_{35}Alm_{41}Gr_{24}$	$Mg_{43}Fe_{12}Ca_{45}$	$Py_{43}Alm_{35}Gr_{22}$	$Mg_{42}Fe_{13}Ca_{45}$	$Py_{77}Alm_{15}Gr_8$	$Mg_{61}Fe_7Ca_{33}$

(Continued)

to the original Superior Province sanukitoid (RR-07), demonstrates that additional assimilation of ultramafic material by Mg-rich diorite liquids is possible, and leads to melts with much higher Mg-numbers (>0·70) without any change in the garnet clinopyroxenite mineral assemblage, but with the single phases (gt and Cpx) becoming progressively more magnesian. In the TTG melt–peridotite assimilation experiments (Table 2: ST/DPl, ST/DP2, ST/DSP3 and CF-HP), liquids with moderate to high Mg-numbers (~0·55–0·77) coexist with garnet websterite (gt + Cpx + Opx) or garnet orthopyroxenite (gt + Opx) residues, with the proportion of garnet again subordinate

Table 3: Continued

Sample:	ST/DP	ST/DP-1	ST/DP1	ST/DP2	ST/DP2	ST/DP3	ST/DP3	CF-HP
P (GPa):	3·5	3·5	3·5	3·5	3·5	3·8	3·8	3·0
T (°C):	1150	1150	1150	1200	1200	1200	1200	1100
Phase:	gt	Opx	Cpx	gt	Cpx	gt	Opx	gt
wt % oxide								
SiO_2	41·89(0·42)	57·49(0·35)	56·49	40·33	54·48	43·52	57·19(0·22)	42·01
TiO_2	0·19(0·03)	0·03(0·005)	0·21	0·24	0·59	0·07	0·013(0·006)	0·51
Al_2O_3	23·17(0·12)	2·34(0·25)	11·29	20·76	17·35	21·55	1·71(0·06)	23·00
FeO*	10·30(1·33)	6·35(0·23)	4·03	23·27	3·98	7·61	5·81(0·09)	10·60
MnO	0·21(0·03)	0·08(0·03)	0·10	0·50	0·06	0·19	0·07(0·02)	0·03
MgO	21·34(1·60)	33·30(0·52)	13·99	11·01	5·22	23·27	35·00(0·22)	19·49
CaO	2·79(0·74)	0·51(0·04)	6·52	9·18	8·99	2·79	0·54(0·01)	5·01
Na_2O	0·13(0·01)	0·74(0·10)	6·19	0·11	8·09	0·10	0·50(0·04)	0·08
K_2O	0·02(0·01)	0·002(0·003)	b.d.	0·008	0·01	b.d.	0·013(0·007)	b.d.
P_2O_5	0·06(0·02)	0·02(0·01)	b.d.	0·12	0·53	0·04	b.d.	0·15
Cr_2O_3	0·17(0·10)	0·16(0·05)	n.a.	n.a.	n.a.	0·62	0·17(0·04)	0·27
Total	100·28	101·19	98·82	99·87	99·29	99·75	101·02	101·46
Mg-no.	0·79	0·93	0·87	0·46	0·78	0·85	0·91	0·77
	$Py_{73}Alm_{20}Gr_7$	$En_{93}Fs_{07}$	$Mg_{67}Fe_{11}Ca_{22}$	$Py_{77}Alm_{15}Gr_8$	$Mg_{61}Fe_7Ca_{33}$	$Py_{78}Alm_{14}Gr_7$	$En_{91}Fs_{09}$	$Py_{67}Alm_{20}Gr_{12}$

Sample:	CF-HP	CF-HP	CF-HP	Mats	Mats	Mats	Mats	Mats
P (GPa):	30	30	30	—	—	—	—	—
T (°C):	1100	1100	1100	—	—	—	—	—
Phase:	Cpx	Opx	phlog	oliv	gt	Cpx	Opx	phlog
wt % oxide								
SiO_2	55·22	56·58	47·63	39·84	39·71	52·67	56·71	39·14
TiO_2	0·16	0·05	1·15	0·013	b.d.	0·07	0·04	0·38
Al_2O_3	6·92	2·54	13·21	b.d.	21·63	2·83	0·91	13·14
FeO*	4·32	8·06	9·21	8·48	7·56	2·79	5·07	3·17
MnO	0·14	0·12	0·05	0·096	0·32	0·08	0·10	0·02
MgO	15·94	32·00	11·89	52·49	21·63	17·06	36·93	26·57
CaO	13·47	0·86	0·48	0·03	5·70	19·72	0·47	0·01
Na_2O	3·56	0·39	4·73	0·003	0·03	2·24	0·16	0·23
K_2O	0·02	b.d.	7·11	0·03	0·01	0·02	0·01	12·57
P_2O_5	0·05	b.d.	0·07	0·03	0·06	b.d.	b.d.	0·005
Cr_2O_3	0·46	0·19	0·004	0·16	4·75	1·92	0·32	0·70
Total	100·25	100·89	95·55	100·98	100·99	99·42	100·72	95·94
Mg-no.	0·87	0·88	0·70	0·92	0·84	0·92	0·93	0·94
	$Mg_{57}Fe_9Ca_{35}$	$En_{88}Fs_{12}$	—	$Fo_{92}Fa_{08}$	$Py_{72}Alm_{14}Gr_{14}$	$Mg_{52}Fe_5Ca_{43}$	$En_{93}Fs_{07}$	—

Starting material for experiments as follows: KJ-2, KJ-3 and KJ-4, Roaring River sanukitoid + ~6–8 wt % H_2O; KJ-6, sanukitoid + H_2O + 15% depleted peridotite; ST/DP experiments, sanukitoid + depleted peridotite in percentage indicated; CF-HP, piston-cylinder experiment conducted at the Laboratoire Magmas et Volcan in Clermont-Ferrand; starting materials were 1:1 mix of TTG SV-4 and depleted peridotite. The numbers in parentheses represent ±1 standard deviation of the mean value in the EPMA analyses; b.d., below detection; n.a., not analyzed.

to that of the pyroxenes. The 'melt-hybridized' phase assemblages formed in these experiments are the products of reactions that stabilize orthopyroxene while consuming all of the original peridotitic olivine at moderate temperatures (~1200°C) and intermediate melt:rock ratios (from ~1:2 to ~1:1). These assemblages can be genetically linked to primary high-Mg dioritic (sanukitoid) or andesitic (HMA) magmas that formed in response to

Table 4: Trace element abundances (ppm) in experimental melts and mineral phases, measured by laser-ablation ICP-MS

Expt.:	KJ2	KJ3	KJ4	KJ6	STDP-1	STDP-2	STDP-3	CF-HP
Melts	($n=2$)	($n=2$)	($n=4$)	($n=5$)	($n=3$)	($n=3$)	($n=4$)	($n=4$)
P	3188	3355	4917(370)	3142(80)	1063(12)	3259(74)	1141(146)	1748(36)
Sc	6·01	3·35	4·55(0·10)	4·95(0·15)	4·32(0·03)	4·26(0·01)	6·43(0·38)	4·38(0·07)
Ti	*3480*	*4320*	*5700*	*3240*	*2771(21)*	*3960*	*1980*	*4140*
V	46·4	8·01	11·7(1·2)	30·8(0·2)	11·5(0·2)	18·5(0·6)	35·1(3·0)	36·2(0·5)
Cr	13·5	5·36	7·8(1·3)	120(4)	88·1(2·2)	18·8(1·2)	217(36)	179(4)
Ni	25·3	0·56	1·07(0·08)	7·5(0·2)	9·02(0·23)	1·18(0·38)	59·4(6·9)	47·0(0·8)
Rb	29·4	36·9	53·3(4·9)	34(2)	138(2)	37·7(1·7)	89·9(7·8)	137(1)
Sr	1755	2179	3001(177)	1829(19)	1159(3)	1927(21)	993(119)	1029(18)
Y	10·6	7·58	9·8(0·8)	8·1(0·1)	3·25(0·10)	7·04(0·32)	3·29(0·33)	4·98(0·13)
Zr	153	74·8	101(5)	531(7)	287(3)	169(2)	268(33)	301(3)
Nb	2·93	3·27	4·60(0·50)	2·89(0·08)	9·39(0·10)	3·25(0·1)	5·03(0·82)	8·69(0·20)
Ba	2018	2608	3441(163)	2011(21)	1033(5)	2269(11)	863(156)	336(7)
La	116	70·8	96·4(5·8)	68·2(0·5)	32·1(0·1)	90·3(1·3)	37·4(6·9)	37·7(0·7)
Ce	121	141	189(3)	111(2)	71·4(1·2)	195(4)	71(10)	81(1)
Nd	56·2	64·5	86·2(1·6)	55·7(1·3)	30·3(0·1)	68·4(1·0)	28·6(2·6)	32·1(0·4)
Sm	9·43	9·91	14·6(1·4)	9·86(0·16)	4·53(0·16)	10·12(0·1)	3·30(0·25)	5·02(0·20)
Eu	2·73	2·78	3·84(0·13)	2·80(0·12)	1·08(0·02)	2·99(0·12)	0·94(0·11)	1·37(0·07)
Gd	6·31	6·58	8·51(0·67)	5·80(0·41)	2·26(0·07)	5·61(0·20)	1·92(0·50)	3·00(0·19)
Dy	2·40	1·93	2·60(0·08)	2·15(0·07)	0·87(0·03)	1·79(0·04)	0·74(0·20)	1·36(0·16)
Er	0·74	0·50	0·75(0·13)	0·43(0·08)	0·24(0·02)	0·48(0·03)	b.d.	0·34(0·08)
Yb	0·69	0·26	0·35(0·09)	0·25(0·02)	0·16(0·01)	<0·3	b.d.	0·23(0·03)
Hf	2·52	1·57	2·09(0·22)	9·70(0·24)	7·89(0·03)	3·27(0·04)	6·65(1·32)	6·13(0·15)
Ta	0·19	0·14	0·20(0·02)	0·217(0·006)	0·61(0·02)	0·14(0·02)	0·32(0·06)	0·32(0·02)
Pb	29·0	1·02	1·41(0·08)	2·63(0·09)	3·2(0·8)	2·16(0·48)	5·53(1·39)	63·2(1·3)
Th	1·89	2·11	2·68(0·25)	1·99(0·08)	7·43(0·08)	1·72(0·07)	4·09(0·72)	0·86(0·10)
U	0·42	0·32	0·46(0·07)	0·85(0·04)	1·78(0·03)	0·45(0·02)	1·75(0·42)	1·29(0·06)

Expt. mineral:	KJ2	KJ3	KJ4	KJ4	KJ6	KJ6	ST/DP1	ST/DP2
Phase:	Cpx	Cpx	Cpx	gt	Cpx	gt	Cpx	Cpx
	($n=4$)	($n=3$)	($n=6$)	($n=3$)	($n=3$)	($n=3$)	($n=2$)	($n=3$)
K	146(30)	n.a.	n.a.	~665	96(35)	~105	670(18)	~262
P	118(26)	212(3)	238(25)	2606(65)	93·7(14·3)	437(37)	85·4(1·5)	118(30)
Sc	11·0(0·5)	9·69(0·32)	7·37(0·19)	52·6(1·7)	6·7(0·5)	25·2(1·0)	5·94(0·08)	8·12(0·42)
V	106(7)	162(11)	149(14)	95·6(1·8)	133(6)	76(6)	121(3)	160(13)
Cr	1079(40)	463(93)	445(49)	643(24)	784(33)	2435(963)	1139(233)	296(94)
Ni	79(14)	20·7(2·7)	27·1(5·5)	10·5(0·1)	40(7)	17·4(2·7)	120(5)	8·48(0·21)
Rb	0·18(0·05)	~0·25	~0·33	1·17(0·03)	<0·3	<0·4	2·1(0·1)	89·9(7·8)
Sr	172(4)	326(7)	314(34)	~12	241(3)	~10	109(4)	167(7)
Y	2·98(0·28)	2·78(0·31)	2·27(0·36)	78·4(1·2)	2·92(0·44)	20·2(2·6)	1·65(0·07)	1·69(0·10)
Zr	8·17(0·65)	4·87(0·28)	4·36(0·65)	29·4(3·5)	26·8(5·6)	75(17)	21·5(0·2)	8·54(1·04)
Nb	~0·02	~0·06	~0·14	~0·30	<0·1	<0·1	0·25(0·02)	<0·11
Ba	2·15(0·10)	~13	7·8(3·8)	~3	<1·1	~1·3	5·0(1·8)	<0·2
La	1·77(0·14)	1·52(0·04)	1·55(0·31)	~0·019	1·81(0·13)	~0·1	1·34(0·03)	1·93(0·62)
Ce	4·00(0·31)	5·76(0·25)	5·33(1·16)	~0·6	6·06(0·38)	1·06(0·28)	4·74(0·13)	6·52(1·00)
Nd	4·62(0·32)	6·17(0·64)	5·64(1·02)	12·9(0·8)	7·0(1·0)	2·66(0·58)	4·40(0·31)	4·85(1·48)
Sm	1·75(0·23)	1·69(0·29)	1·66(0·12)	8·9(2·2)	2·53(0·90)	1·38(0·28)	0·86(0·03)	1·07(0·04)
Eu	0·58(0·12)	0·72(0·08)	0·66(0·12)	5·5(0·1)	0·84(0·10)	0·83(0·23)	0·30(0·03)	0·40(0·11)
Gd	1·45(0·05)	1·08(0·08)	1·30(0·10)	15·8(4·0)	1·29(0·34)	3·90(0·50)	0·91(0·08)	<0·9
Dy	0·61(0·11)	0·60(0·03)	0·81(0·10)	13·35(0·87)	0·94(0·11)	3·90(0·22)	0·40(0·04)	<0·6
Er	0·34(0·12)	<0·2	<0·3	9·11(0·11)	<0·3	1·93(31)	b.d.	<0·5
Yb	~0·2	~0·23	~0·6	6·34(0·13)	<0·4	1·69(0·23)	0·21(0·03)	<0·4
Hf	0·37(0·04)	~0·32	<0·4	<1·5	~1·0	1·50(0·15)	0·93(0·23)	<0·1
Ta	<0·02	~0·08	~0·08	<0·3	<0·1	<0·1	b.d.	<0·1
Pb	0·47(0·05)	<0·2	<0·2	<0·2	<0·6	<0·6	b.d.	<0·6
Th	<0·1	<0·2	<0·3	<0·4	<0·1	<0·1	0·22(0·02)	<0·1
U	<0·05	<0·1	<0·1	<0·1	<0·1	b.d.	~0·06	<0·1

(Continued)

Table 4: Continued

Expt. mineral:	ST/DP2	ST/DP3	CF-HP	CF-HP
Phase:	gt	gt	gt	Cpx
	($n=3$)	($n=2$)	($n=3$)	($n=1$)
K	~75	~74	n.a.	31·6
P	955(23)	235(92)	321(48)	45·4
Sc	57·8(1·3)	38(3)	n.a.	10·54
V	113(6)	96(3)	77(5)	136
Cr	772(91)	7480(778)	5681(704)	3927
Ni	4·3(1·5)	139(16)	225(20)	343
Rb	<0·5	0·49(0·35)	<0·8	b.d.
Sr	5·9(0·6)	~5·8	1·7(0·02)	126
Y	71(0·9)	11·8(1·7)	44(8)	2·78
Zr	66(11)	60·7(9·7)	141(8)	22·9
Nb	<0·11	0·15(0·02)	0·13(0·04)	0·04
Ba	<1·5	7·2(1·6)	~0·7	1·59
La	<0·3	~0·1	0·07(0·03)	1·67
Ce	2·56(0·18)	~0·12	0·50(0·09)	7·93
Nd	9·3(0·1)	~0·33	1·69(0·05)	8·28
Sm	4·8(0·1)	0·87(0·03)	0·49(0·04)	2·35
Eu	3·00(0·23)	0·28(0·06)	1·07(0·16)	0·72
Gd	12·2(1·7)	1·47(0·27)	4·95(0·15)	1·76
Dy	12·0(1·1)	1·82(0·18)	6·41(0·57)	0·77
Er	6·45(0·28)	1·51(0·10)	4·34(0·62)	0·28
Yb	6·17(0·88)	1·72(0·05)	4·56(0·35)	b.d.
Hf	<1·1	0·95(0·23)	2·23(0·09)	1·11
Ta	<0·1	<0·03	<0·05	b.d.
Pb	<0·8	0·21(0·10)	0·86(0·09)	2·74
Th	<0·14	0·07(0·03)	<0·12	b.d.
U	<0·1	~0·04	<0·06	b.d.

Expt. mineral:	ST/DP1	ST/DP2	ST/DP3	CF-HP	Matsoku
Phase:	Opx	Opx	Opx	Opx	Opx
	($n=1$)	($n=2$)	($n=5$)	($n=1$)	($n=3$)
P	*41·3*	13·8(6·5)	19·0(4·1)	29·3	13·6(1·1)
K	9·95	12·1	—	47·1	63·8
Sc	*2·86*	2·52(0·13)	3·11(0·25)	4·19	2·96(0·07)
Ti	*202*	74·3(3·1)	71·6(6·5)	328	188(8)
V	*44·5*	32(3)	32·8(1·9)	37·2	39(1)
Cr	*1323*	1195(108)	1194(383)	1736	2379(102)
Ni	*217*	521(69)	641(72)	671	957(16)
Sr	*2·81*	0·99(0·71)	1·50(0·57)	1·2	0·45(0·17)
Y	*0·23*	0·12(0·05)	0·10(0·03)	0·32	0·04(0·01)
Zr	*1·70*	1·01(0·47)	0·78(0·30)	1·62	0·61(0·04)
Nb	*0·02*	*0·12*	—	*0·07*	0·12(0·01)
Ba	0·86	0·64	—	1·01	0·12
La	*0·04*	*0·04*	*0·17*	—	0·01
Ce	*0·19*	*0·11*	*0·11*	0·09	0·04(0·01)
Nd	*0·25*	*0·15*	—	0·21	0·06(0·02)
Sm	*0·08*	—	—	—	—
Eu	*0·02*	—	—	—	—
Gd	*0·09*	—	*0·52*	0·15	*0·01*
Dy	—	—	—	0·21	*0·02*
Er	—	—	*0·22*	*0·19*	*0·02*
Yb	—	—	—	0·23	—
Hf	*0·07*	—	—	0·13	*0·03*
Ta	—	—	—	—	*0·02*
Pb	—	*0·54*	—	*0·88*	*0·02*
Th	*~0·01*	*<0·03*	—	—	—
U	—	*<0·06*	—	—	—

na., not analyzed; data preceded by ~ denote elements for which only a single analysis was above the detection limit; data preceded by '<' denote elements at concentrations 'below the detection limit' (given by the number that follows). The numbers in parentheses represent ±1 standard deviation of the mean value in the laser-ablation analyses; italicized values represent EPMA measurement for titanium (Ti); b.d., below detection; n.a., not analyzed.

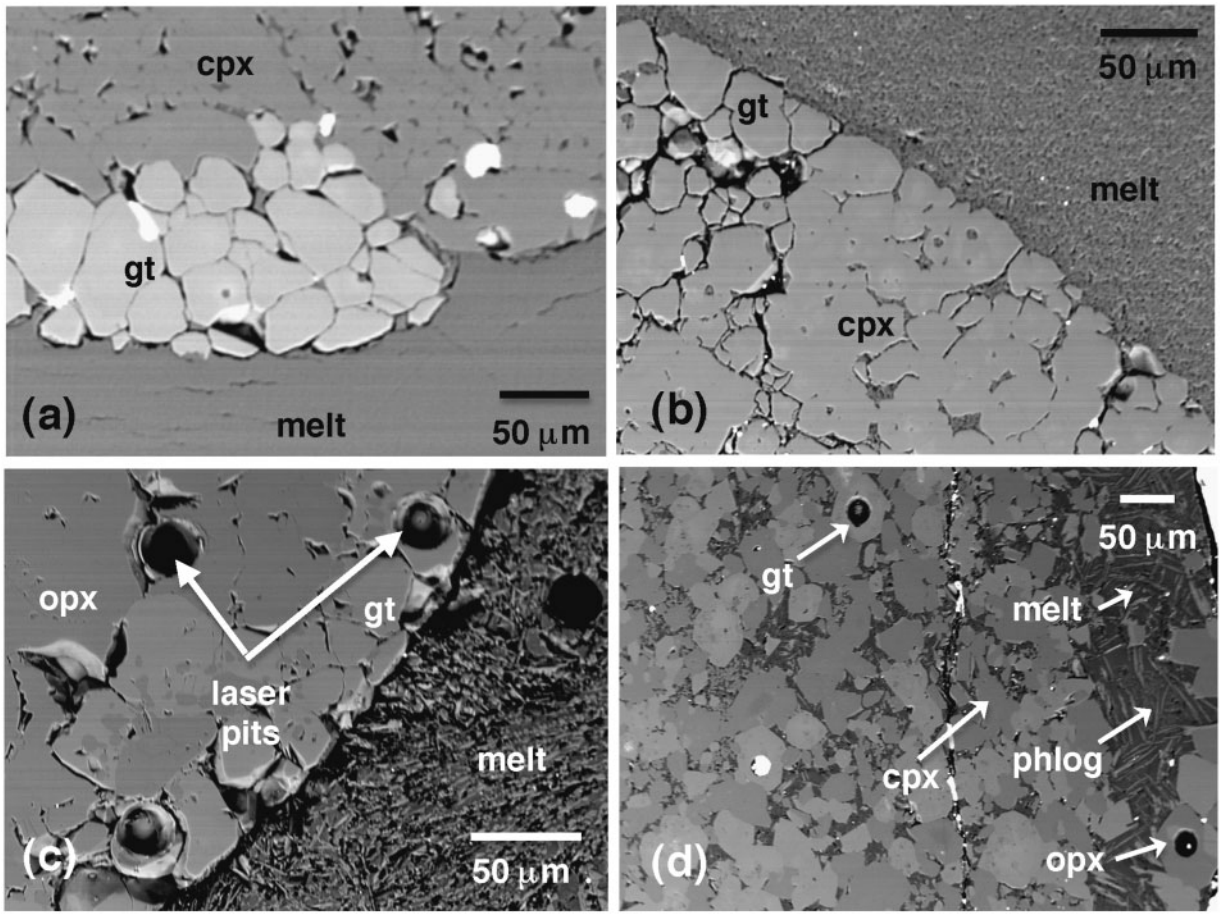

Fig. 2. Back-scattered electron photomicrographs of typical experimental melt + mineral phase assemblages. (a) Experiment KJ-3, sanukitoid near-liquidus experiment with RR-07 starting material, 3·8 GPa, 1200°C; (b) experiment KJ6, peridotite assimilation experiment with sanukitoid RR-07 + ~30% depleted peridotite AVX-51, 3·8 GPa, 1250°C; (c) peridotite assimilation experiment ST/DP2, sanukitoid ST-01 + 30% depleted peridotite AVX-51, 3·8 GPa, 1200°C, showing craters from laser-ablation ICP-MS analyses; (d) peridotite assimilation experiment CF-HP, TTG SV-4 + 30% depleted peridotite 8710P, run in piston-cylinder apparatus at 3·0 GPa, 1100°C.

reaction between hydrous tonalite or sanukitoid melts and depleted peridotite. At lower pressures and/or temperature (e.g. from this study, experiment CF-HP: ~3·0 GPa, 1100°C), these 'melt-metasomatized' reaction assemblages also contain phlogopite and/or amphibole (e.g. Sen & Dunn, 1994*b*; Yaxley & Green, 1998; Rapp *et al.*, 1999).

Melt compositions

The silicate liquids produced in our experiments are all quartz normative, with K_2O/Na_2O close to or greater than 1·0, and in terms of their CIPW normative composition can be classified as quartz monzodiorite, quartz monzonite, or monzodiorite, according to Streckeisen (1976). Near-liquidus sanukitoid melts (experiments KJ-2, KJ-3, and KJ-4) have Mg-numbers (~0·46 to 0·53) that are slightly lower and SiO_2 concentrations (62–66 wt %, on an anhydrous basis) that are slightly higher than the initial bulk composition (Mg-number = 0·61, SiO_2 58·53 wt %) (Fig. 3), in accord with the proportion of near-liquidus crystalline phases (lowest in KJ-2, at ~28% crystals). The 'mantle-hydridized' TTG melts of the assimilation experiments (KJ-6, ST-DP1, ST/DP2, ST/DP3, and CF-HP) have higher Mg-numbers (~0·49 to 0·77) and lower SiO_2 contents (58–66 wt %) relative to (1) their respective original tonalitic starting compositions (SV4, RR-07 and ST-01; see Table 1), (2) experimental melts of hydrous metabasalt at ~1–4 GPa (Sen & Dunn, 1994*a*; Rapp & Watson, 1995), and (3) Archean TTG (Fig. 3). Thus in terms of Mg-number and wt % SiO_2, the experimental melts are closely comparable with parental Late Archean sanukitoids; some melts extend further still to the higher Mg-numbers characteristic of high-magnesium andesites (HMAs; see Rogers & Saunders, 1989; Tatsumi *et al.*, 2003, Tsuchiya *et al.*, 2005; Tatsumi, 2006; Gomez-Tuena *et al.*,

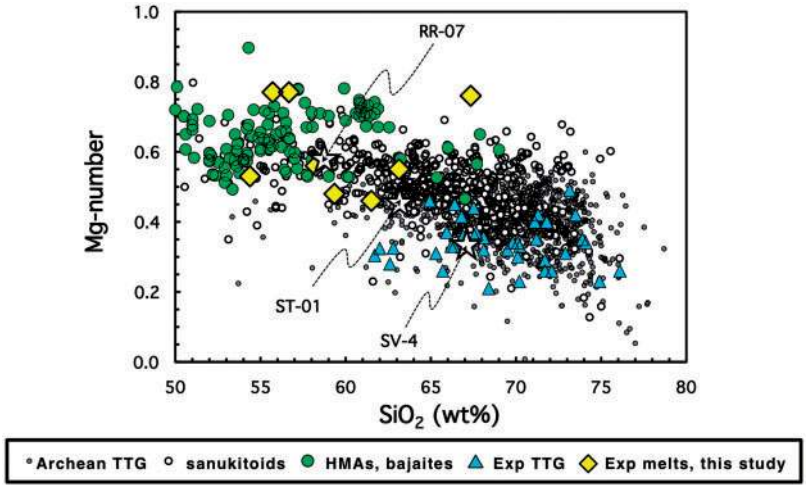

Fig. 3. Mg-number vs wt % SiO_2 for experimental high-Mg diorite melts and granitoid starting materials SV-4 (TTG), ST-01 and RR-07 (sanukitoids), shown relative to Archean TTG, Late Archean sanukitoids, high-magnesian andesites (HMAs) and bajaites from modern subduction zone settings, and experimental 'TTG' melts produced by dehydration melting of garnet-amphibolite and eclogite at 1–3 GPa (Rapp *et al.*, 1991; Sen & Dunn, 1994*a*; Rapp & Watson, 1995).

2007) and bajaites (see Rogers *et al.*, 1985; Saunders *et al.*, 1987; Benoit *et al.*, 2002; Calmus *et al.*, 2003) from modern subduction zones (Fig. 3).

In spite of the varied P–T conditions and residual phase assemblages, the primitive mantle (PM) normalized trace element abundance patterns of the experimental liquids as a group are generally parallel to each other, with their overall shape closely resembling those of the granitoid components of the experimental starting materials (Fig. 4). For example, in Fig. 4 the pattern for the SV-4 TTG starting material (Mg-number = 0·37; SiO_2 66·44 wt %) can be directly compared with its mantle-hybridized counterpart (experiment CF-HP; Mg-number = 0·56; SiO_2 58·24 wt %); the two trends display an overall parallelism, with higher concentrations of most trace elements [except for the heavy rare earth elements (HREE) and Y, because of the presence of garnet] in the experimental 'sanukitoid' melt, as a consequence of the 'dilution' effect of the assimilation reaction, and elevated Cr, Ni and V contents. Common features of all the experimental liquids include positive anomalies in K, Pb (see qualification below), and V relative to neighboring elements in Fig. 4, and negative anomalies in Th, U, Nb, Ta, Ti, and Sc relative to primitive mantle abundances. The often-noted pairing of high Sr/Y and $(La/Yb)_N$ ratios with strong relative depletions in Y and HREE (e.g. Yb), respectively, characteristic features of Archean TTG and sanukitoids, remain intact following the assimilation reaction.

Of particular interest is the contrasting behavior of lead (Pb) in different experiments, depending upon which noble metal sample capsule was used. For experiments carried out in thick-walled gold capsules, Pb concentrations in the melt are unexpectedly low (~1–5 ppm; Table 2), leading us to suspect that these experiments have been affected by Pb loss to the capsule, primarily from the melt phase (experiment KJ2, which appears to have experienced only partial Pb loss, is an exception, for unknown reasons). However, in the single experiment carried out with a thick-walled capsule of Au_{80}–Pd_{20} alloy (CF-HP), Pb concentrations in the melt are more than an order of magnitude higher (~63 ppm), leading us to believe that Pb loss in this run has been suppressed. The data for Pb from this experiment are used to estimate new mineral–melt distribution coefficients (D values) for Pb for garnet and clinopyroxene in equilibrium with Mg-rich dioritic melts (sanukitoids).

Mineral compositions (major elements)

The major and trace element compositions of experimental garnet, clinopyroxene, orthopyroxene and phlogopite are listed in Tables 4 and 5. The compositions of coexisting garnet (gt) and clinopyroxene (Cpx) representative of the two types of experiments are shown in a ternary diagram of molar Mg–Fe–Ca (Fig. 5), with garnet, and to a lesser extent clinopyroxene, showing a range of compositions that fall along a trend extending from the more Fe-rich compositions of the sanukitoid liquidus experiments to the more Mg-rich compositions of the peridotite assimilation experiments. The Ca–Fe–Mg compositions of garnet and clinopyroxene in the sanukitoid liquidus experiments are comparable with those of 'crustal' eclogite residues of basalt dehydration melting at ~1·6–3·2 GPa that are in equilibrium with TTG-like liquids (Rapp & Watson, 1995). These eclogites correspond to the 'Group B' eclogites of

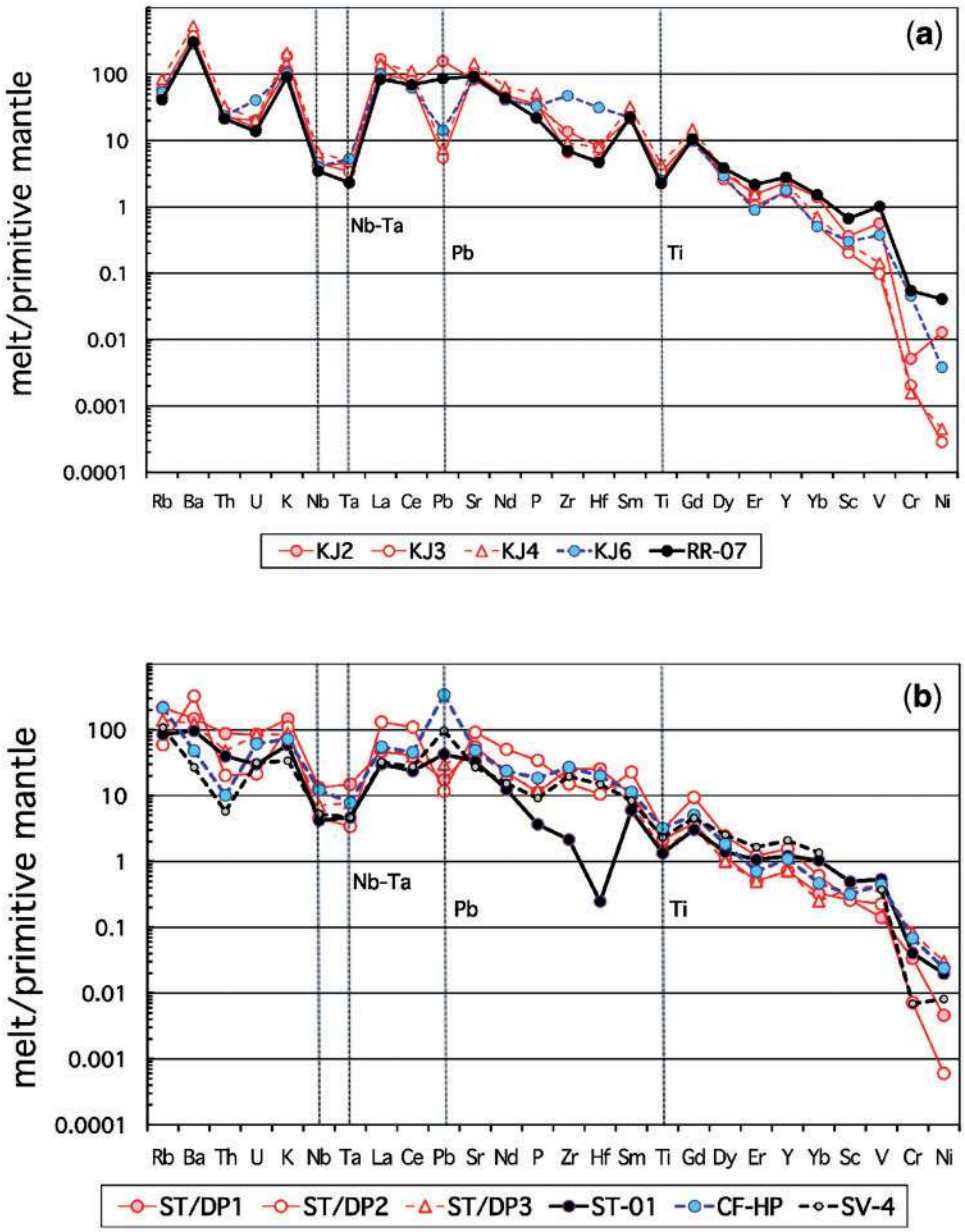

Fig. 4. Trace element abundance patterns for experimental melts, including RR-07 sanukitoid near-liquidus experiments (KJ2, KJ3, KJ4), RR-07 sanukitoid–peridotite assimilation (KJ6), Saganaga Tonalite + peridotite assimilation (ST/DP1, ST/DP2, ST/DP3), and SV-4 TTG + peridotite assimilation (CF-HP), shown relative to patterns for granitoid experimental starting materials (SV-4; RR-07; ST-01), all normalized to primitive mantle abundances of Sun & McDonough (1989). The negative anomaly in Pb in most of the experimental melts is due to preferential loss of Pb to the gold sample capsule; the melt in experiment KJ2 appears to have undergone only partial Pb loss. The positive anomaly in Pb in the melt from experiment CF-HP is considered to represent the equilibrium concentration; this experiment was carried out using Au–Pd alloy capsule, which does not appear to be susceptible to Pb loss. Other notable negative anomalies are observed for niobium–tantalum and titanium. The very low Zr and Hf measured in the ST-01 starting material (panel B) may be due to undissolved zircon during the solution ICP-MS bulk analysis.

Taylor & Neal (1989), Sobolev *et al.* (1999), and Taylor *et al.* (2003). Garnet and clinopyroxene products of reaction between peridotite and TTG melts are richer in the Mg-component, and are similar in composition to gt and Cpx in 'Group A' eclogites and websterites (Taylor *et al.*, 2003), members of an 'intermediate' or 'websteritic' paragenesis transitional between Group B eclogites and garnet peridotites (Sobolev *et al.*, 1999). In our experiments, liquids with moderate to very high Mg-numbers coexist with reaction residues resembling these parageneses

Table 5: Experimentally determined mineral–melt D *values for garnet, clinopyroxene, and orthopyroxene in equilibrium with Mg-rich diorite (sanukitoid) melts*

	Garnet					
Sample:	KJ4	KJ6	ST/DP2	ST/DP3	CF-HP	FSS-3.2
Rb	0·022	b.d.	0·015	0·0027	b.d.	0·0073
Ba	0·0008	0·00065	b.d.	0·00014	0·0021	0·0026
Th	b.d.	b.d.	b.d.	0·024	b.d.	0·0410
U	b.d.	b.d.	b.d.	0·04	b.d.	0·1104
K	b.d.	0·0041	0·0027	0·0015	b.d.	0·0024
Nb	0·0634	0·0346	b.d.	0·0354	0·0149	0·6603
Ta	b.d.	b.d.	b.d.	b.d.	b.d.	*0·9*
La	0·0002	0·0015	b.d.	0·0055	0·0019	0·0066
Ce	0·003	0·0095	0·0131	0·0024	0·0062	0·0270
Pb	b.d.	b.d.	b.d.	0·0036	0·0136	0·0050
Sr	0·0039	0·0056	0·0031	0·00055	0·0017	0·0021
Nd	0·1484	0·0478	0·1359	0·01084	0·0527	0·3367
P	0·5377	0·1391	0·2930	0·1902	0·1836	0·9070
Zr	0·2854	0·1412	0·3905	0·2265	0·4684	1·2665
Hf	b.d.	0·1546	b.d.	0·3308	0·3638	0·8415
Sm	0·6224	0·1340	0·4753	0·4545	0·2968	1·82
Ti	0·2	0·4259	0·3636	0·2121	0·7391	3·326
Gd	1·787	0·6724	2·180	0·7656	1·65	5·727
Dy	5·056	1·814	6·687	1·986	4·706	16·38
Er	12·15	4·489	13·44	b.d.	12·76	32·33
Y	7·686	2·494	10·085	3·861	8·835	22·22
Yb	18·12	6·76	20·57	b.d.	19·826	43·5
Sc	11·56	5·091	13·57	5·910	b.d.	18·74
V	8·171	2·468	6·108	2·934	2·127	26·74
Cr	156·8	20·29	41·06	34·99	31·74	109
Ni	11·93	2·32	3·644	1·835	4·787	37·04

	Clinopyroxene						
Sample:	KJ2	KJ3	KJ4	KJ6	ST/DP1	ST/DP2	CF-HP
Rb	0·0034	0·0068	0·0062	b.d.	0·0152	0·0080	b.d.
Ba	0·001085233	0·005	0·002076677	b.d.	0·0048	b.d.	0·0047
Th	b.d.	b.d.	b.d.	b.d.	b.d.	b.d.	b.d.
U	b.d.	b.d.	b.d.	b.d.	b.d.	b.d.	b.d.
K	0·0067	b.d.	0·0073	0·0037	0·0183	0·0096	0·0017
Nb	0·007	0·0183	0·0296	b.d.	0·0266	b.d.	0·0046
Ta	b.d.	b.d.	b.d.	b.d.	b.d.	b.d.	b.d.
La	0·0153	0·0215	0·0157	0·0265	0·0417	0·0214	0·0443
Ce	0·0331	0·0409	0·0267	0·0546	0·0664	0·0334	0·098
Pb	b.d.	b.d.	b.d.	b.d.	b.d.	b.d.	0·0434
Sr	0·0980	0·1496	0·1027	0·1318	0·094	0·0866	0·1224
Nd	0·0822	0·0957	0·0649	0·1257	0·1452	0·0709	0·258
P	0·0370	0·0632	0·0492	0·0298	0·0803	0·0362	0·026
Zr	0·0534	0·0651	0·0423	0·0505	0·075	0·0505	0·0761
Hf	0·1468	0·2038	b.d.	0·1031	0·118	b.d.	0·1811
Sm	0·1856	0·1705	0·1161	0·2566	0·19	0·1057	0·4681
Ti	0·2158	0·4028	0·3158	0·2407	0·5	0·8939	0·2319
Gd	0·2298	0·1641	0·1471	0·2224	0·403	b.d.	0·5867
Dy	0·2542	0·3109	0·3068	0·4372	0·46	b.d.	0·5662
Er	0·4595	b.d.	b.d.	b.d.	b.d.	b.d.	0·8235
Y	0·2811	0·3668	0·2225	0·3605	0·5077	0·2401	0·5582
Yb	0·3478	0·8846	1·714	b.d.	1·3125	b.d.	b.d.
Sc	1·830	2·893	1·620	1·353	1·375	1·906	2·406
V	2·284	20·22	12·74	4·318	10·52	8·649	3·757
Cr	79·93	86·38	108·5	6·533	12·93	15·75	21·94
Ni	3·123	36·96	30·80	5·333	13·30	7·186	7·3

(Continued)

Table 5: Continued

	Orthopyroxene			
Sample:	ST/DP1	ST/DP2	ST/DP3	CF-HP
Rb				
Ba	0·0008	0·0003		0·003
Th	0·0013	0·0581		
U		0·13		
K	0·0003	0·0004		0·0026
Nb	0·0021	0·037		0·0081
Ta				
La	0·0012	0·0004	0·0045	
Ce	0·0027	0·0006	0·0015	0·0011
Pb		0·25		0·0139
Sr	0·0024	0·0005	0·0015	0·0012
Nd	0·0083	0·0022		0·0065
P	0·0389	0·0042	0·0167	0·0168
Zr	0·006	0·006	0·0029	0·0054
Hf	0·0089			0·0212
Sm	0·0177			
Ti	0·073	0·0188	0·0362	0·0792
Gd	0·0398		0·2708	0·05
Dy				0·1544
Er				0·559
Y	0·0708	0·017	0·0304	0·0643
Yb				1
Sc	0·662	0·5915	0·4837	0·9566
V	3·87	1·73	0·9345	1·03
Cr	15·017	63·6	5·5023	9·7
Ni	24·05	442	10·8	14·276

(garnet pyroxenite and garnet websterite). Clinopyroxenes in both sets of experiments are further characterized by relatively high Na and Al contents and corresponding large jadeite ($NaAlSi_2O_6$) and Ca-Tshermak's ($CaAl[AlSiO_6]$) components.

Orthopyroxene (Opx) plays a critically important role as the primary product phase of the peridotite assimilation reaction, forming as a consequence of the complete consumption of peridotitic olivine. The metasomatic orthopyroxenes produced in reactions between TTG melts and depleted peridotite have variable but generally lower Mg-numbers (~0·88–0·93), and higher CaO (0·5–1·0 wt %) and Al_2O_3 (~1·5–2·5 wt %) contents than most peridotitic orthopyroxenes (occurring as both diamond inclusions or in xenoliths) (Fig. 6a and b). When data for orthopyroxenes formed in other melt–rock reaction or assimilation experiments involving 'tonalitic' liquids and crystalline peridotite (e.g. Johnston & Wyllie, 1989; Carroll & Wyllie, 1989; Sen & Dunn, 1994*b*; Rapp *et al.*, 1999) are included, together with data for cratonic orthopyroxenes of the pyroxenitic and websteritic parageneses [e.g. Opx diamond inclusions from Siberia (Sobolev *et al.*, 1998), Kaapvaal (Aulbach *et al.*, 2002) and Tanzania (Stachel *et al.*, 1998*a*); and Opx in garnet pyroxenite and garnet websterite xenoliths from the Slave Province (Aulbach *et al.*, 2007), Kaapvaal (Simon *et al.*, 2007) and Siberia (Ota *et al.*, 2004)], a general trend of increasing CaO and Al_2O_3 content with decreasing Mg-number is apparent (Fig. 6a and b). The array of experimental orthopyroxene compositions in Fig. 6 appears to be related to the nature of the peridotitic starting material of the experiments [whether fertile lherzolite, in the case of Sekine & Wyllie (1982), Johnston & Wyllie (1989), and Carroll & Wyllie (1989), Sen & Dunn (1994*b*) and Yaxley & Green (1998); or depleted harzburgite, in the case of Rapp *et al.* (1999) and this study], as well as temperature and the melt:rock ratio. For example, the highest temperature experiments with fertile peridotite produce 'metasomatic' orthopyroxene with the highest Mg-numbers, and the highest CaO and Al_2O_3 contents, whereas experiments with the most depleted peridotite at intermediate temperatures produce orthopyroxene with the lowest Mg-numbers. These interdependences warrant more systematic experimental study in the future.

Mineral compositions (trace elements)

Garnet

Laser-ablation data are reported for garnet from four experiments: KJ-4 (sanukitoid liquidus), KJ-6 (sanukitoid liq. + peridotite), and two TTG–peridotite reaction experiments (ST/DP1 and ST/DP3), with the average of 2–5 analyses listed in Table 4. These data are used in two ways: (1) for comparisons with natural samples of cratonic garnet occurring as diamond inclusions and in peridotite and pyroxenite xenoliths, to assess the role that melt–rock reaction may have played in the chemical evolution of the SCLM; (2) in combination with trace element data for the experimental mantle-hybridized melts, to determine mineral–melt distribution coefficients (D values), for use in petrogenetic modelling of melt–rock reaction. Primitive mantle normalized trace element abundance patterns for the experimental garnets are shown in Fig. 7a. There are a number of distinct and persistent trace element characteristics common to all of the experimental garnets in Fig. 7a, including prominent positive anomalies in U, Ta, and Pb relative to neighboring elements, and prominent negative anomalies in Ba, Nb, Sr, Ti and Ni. Chondrite-normalized REE patterns (Fig. 7b) are strongly depleted in light REE (LREE; La, Ce) and flat in the middle REE (MREE) to HREE (~Sm–Yb) at ~20× chondrite; in this respect, they resemble garnets in eclogite xenoliths from the Kaapvaal Craton (Jacob *et al.*, 2003) and garnet inclusions in diamonds from the Siberian

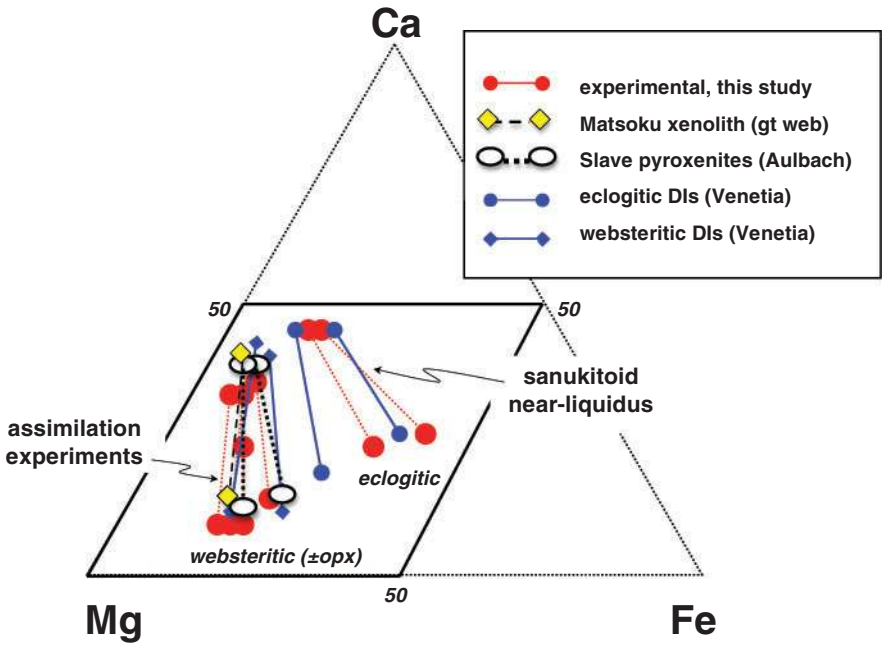

Fig. 5. Ternary Ca–Fe–Mg plot of representative garnet–clinopyroxene pairs from the peridotite assimilation experiments (ST/DP runs) and the sanukitoid near-liquidus experiments (KJ runs). For comparison are shown garnet–clinopyroxene pairs in (1) a garnet websterite xenolith from the Matsoku kimberlite in Lesotho (R. Rapp, this study), garnet pyroxenite xenoliths from the Slave Craton (Aulbach *et al.*, 2007), and eclogitic and garnet websteritic diamond inclusions from the Venetia kimberlite in South Africa (Aulbach *et al.*, 2002). Coexisting garnet–clinopyroxene pairs can be divided into eclogitic ('E-type') and 'intermediate' or websteritic parageneses (Sobolev *et al.*, 1999).

Craton (Ireland *et al.*, 1994), and are readily distinguishable from (predominantly) harzburgitic garnets in diamonds and xenoliths, which possess sinusoidal REE patterns that are generally attributed to fluid metasomatism (Stachel & Harris, 1997; Stachel *et al.*, 1998*b*).

Clinopyroxene

Laser-ablation ICP-MS data are reported for experimental clinopyroxenes from each of the three sanukitoid liquidus experiments (KJ-2, KJ-3, and KJ-4), and for the four experiments in which clinopyroxene was present after sanukitoid or TTG melts had reacted with peridotite (KJ-6, ST/DP1, ST/DP2, and CF-HP); these data are listed in Table 4 and their corresponding primitive mantle normalized trace-element abundance patterns are shown in Fig. 8. As with garnet, the experimental clinopyroxenes show some common, distinctive characteristics, including strong depletion in Nb coupled with low Nb/Ta ratios, Ce/Pb ratios >10 (except when phlogopite is present), positive anomalies in Sr and V and a slight but not universal negative anomaly in Ti, and primitive mantle normalized Sc/V ratios <0·1 and Cr/Ni ratios >10. Chondrite-normalized REE patterns (not shown) are convex, with a maximum at Nd, and a slight enrichment in the LREE relative to the HREE.

Orthopyroxene

Laser-ablation ICP-MS data are reported for experimental orthopyroxenes (Opx) from three experiments (CF-HP, ST/DP2 and ST/DP3; Table 4). For many trace elements, concentrations in Opx in a given experiment are below the detection limit, although a measurable value has been obtained for most elements in orthopyroxene from at least one experiment. The (incomplete) trace element abundance patterns for Opx, normalized to primitive mantle abundances, are shown in Fig. 9. A distinct and prominent positive Pb anomaly is clearly evident, as are strong negative Y anomalies; PM-normalized ratios for Sc/V are <1·0 and for Cr/Ni are >1·0. The prominent Pb and Y anomalies observed in the experimental Opx (produced in the reaction between TTG or sanukitoid melts and peridotite rock), are also apparent in orthopyroxene inclusions in diamonds from the Snap Lake kimberlite (Promprated *et al.*, 2004) and Opx in garnet peridotite xenoliths from the Diavik kimberlite (G. Yaxley, unpublished data), both within the Slave Craton, and in Opx from a garnet websterite xenolith from Matsoku (R. Rapp, this study) and phlogopite-rich mafic xenoliths from the Kimberley area, South Africa, both within the Kaapvaal Craton. Orthopyroxenes in low-temperature peridotite xenoliths from the Kimberley area and northern Lesotho in the Kaapvaal Craton (Simon *et al.*, 2007) show similar

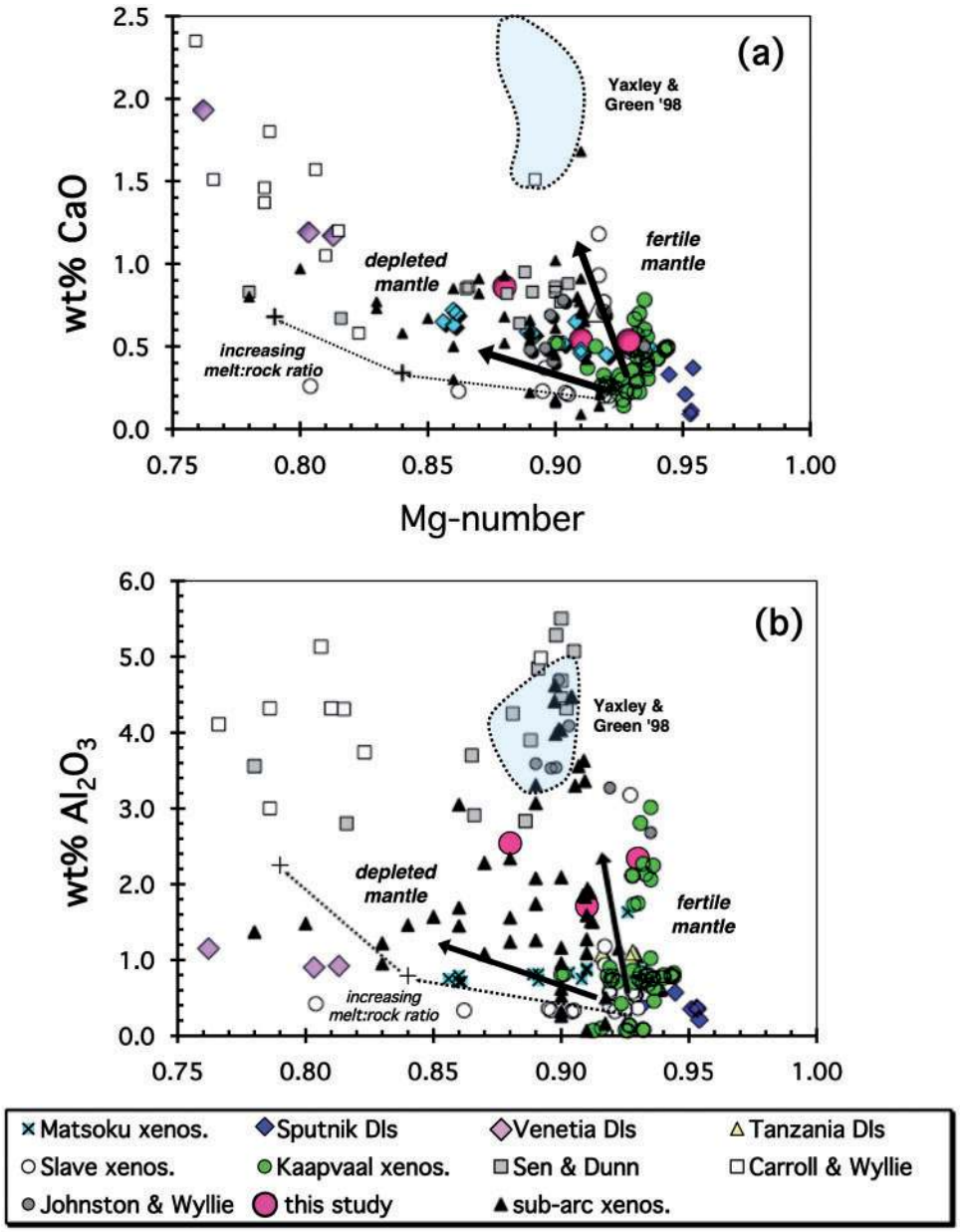

Fig. 6. Compositions of orthopyroxenes in cratonic xenoliths and diamond inclusions, compared with experimental orthopyroxene formed in reactions between granitoid melts and crystalline peridotite, and with orthopyroxene from metasomatized spinel peridotite xenoliths from sub-arc mantle in modern subduction zones, repesented in terms of (a) Mg-number vs wt % CaO, and (b) Mg-number vs wt % Al_2O_3. Data sources for experimental samples: Carroll & Wyllie (1989), Johnston & Wyllie (1989), Sen & Dunn (1994*b*), Yaxley & Green (1998) and Rapp *et al.* (1999). Data sources for orthopyroxene diamond inclusions: Sputnik kimberlite, Siberian Craton, Sobolev *et al.* (1997); Venetia kimberlite, Kaapvaal Craton, Aulbach *et al.* (2002); Mwdui kimberlite, Tanzania, Stachel *et al.* (1998*a*). Data sources for orthopyroxene in cratonic xenoliths: Diavik kimberlite, Slave Craton, Aulbach *et al.* (2007); Kimberley and Lesotho kimberlites, Kaapvaal Craton, Simon *et al.* (2007). Data sources for orthopyroxene in sub-arc mantle xenoliths: Papua, New Guinea, Grégoire *et al.* (2001) and McInness *et al.* (2001); Grenada, Vannucci *et al.* (2007); Philippines, Grégoire *et al.* (2008). Two distinct compositional trends can be defined in the experimental samples, based upon the nature of the peridotite being assimilated or metasomatized; one trend, defined by orthopyroxene formed in reactions between hydrous granitoid melts and depleted peridotite, involves significant decreases in Mg-number coupled with only minor increases in CaO and Al_2O_3 (e.g. Rapp *et al.*, 1999), whereas the other, defined by orthopyroxene formed in reactions between hydrous granitoid melts and fertile peridotite, involves only minor decreases in Mg-number, but large increases in CaO and Al_2O_3 contents (e.g. Yaxley & Green, 1998).

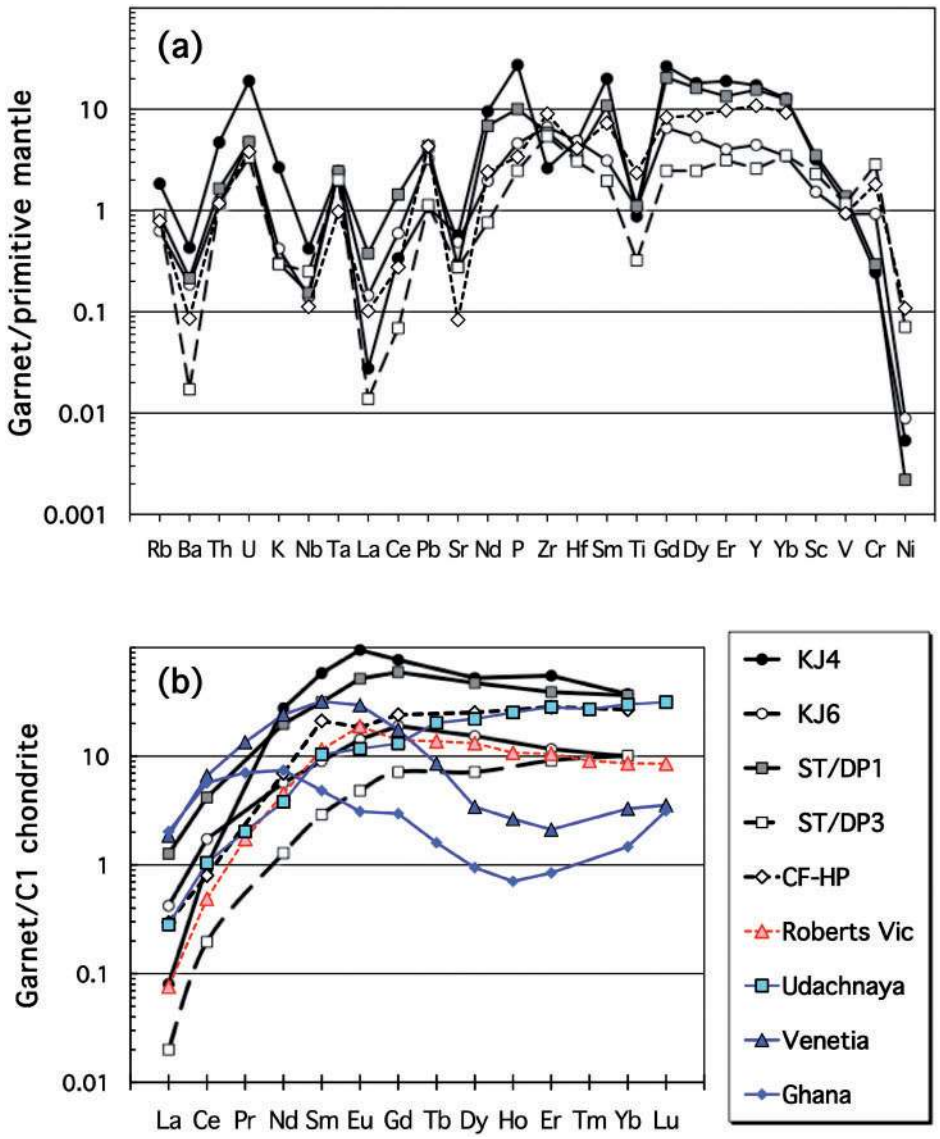

Fig. 7. (a) Trace element abundance patterns for experimental garnets in equilibrium with Mg-rich diorite melts, normalized to primitive mantle, and (b) chondrite-normalized rare earth element (REE) patterns for experimental garnets compared with REE patterns for garnets in eclogitic xenoliths from the Roberts Victor kimberlite, Kaapvaal Craton, South Africa (Jacob *et al.*, 2003) and the Udachnaya kimberlite, Siberian Craton (Jacob *et al.*, 1994); and for garnet diamond inclusions of the harzburgitic paragenesis from Ghana (Stachel & Harris, 1997) and the Venetia kimberlite, Kaapvaal Craton, South Africa (Stachel *et al.*, 2004).

prominent Pb (positive) and Y (negative) anomalies. All of these particular cratonic samples share the low, primitive mantle normalized Sc/V ratios and high Cr/Ni ratios of the experimental Opx. When data for orthopyroxenes in metasomatized spinel peridotite xenoliths from the sub-arc mantle in Papua, New Guinea are included, pronounced Pb and Y anomalies, similar to those seen in the experimental and cratonic orthopyroxenes, are observed, in addition to the high Cr/Ni ratios. However, in contrast to the low Sc/V ratios (normalized to PM) of the experimental and cratonic orthopyroxenes, the orthopyroxenes in the melt-metasomatized sub-arc spinel peridotites have high Sc/V ratios, which might possibly be related to the absence of garnet, with its high PM-normalized Sc/V ratios (see Fig. 7a).

Mineral–melt distribution coefficients (*D* values)

A comprehensive set of mineral–melt distribution coefficients (*D* values; Table 5) specific to equilibria between Mg-rich diorite melts and a garnet pyroxenite phase assemblage can be calculated by combining the

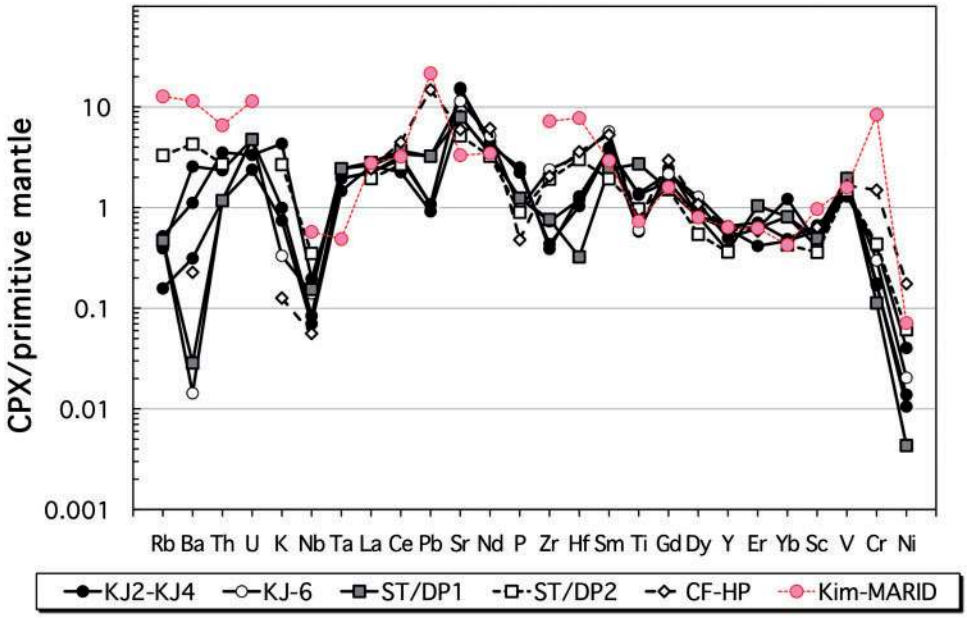

Fig. 8. Trace element abundance patterns for experimental clinopyroxene in equilibrium with Mg-rich diorite melts, normalized to primitive mantle. Also shown is trace element pattern for clinopyroxene coexisting with phlogopite in MARID-type xenolith (Grégoire *et al.*, 2002), analagous to clinopyroxene in CF-HP experiment (note the positive anomaly in Pb in both samples).

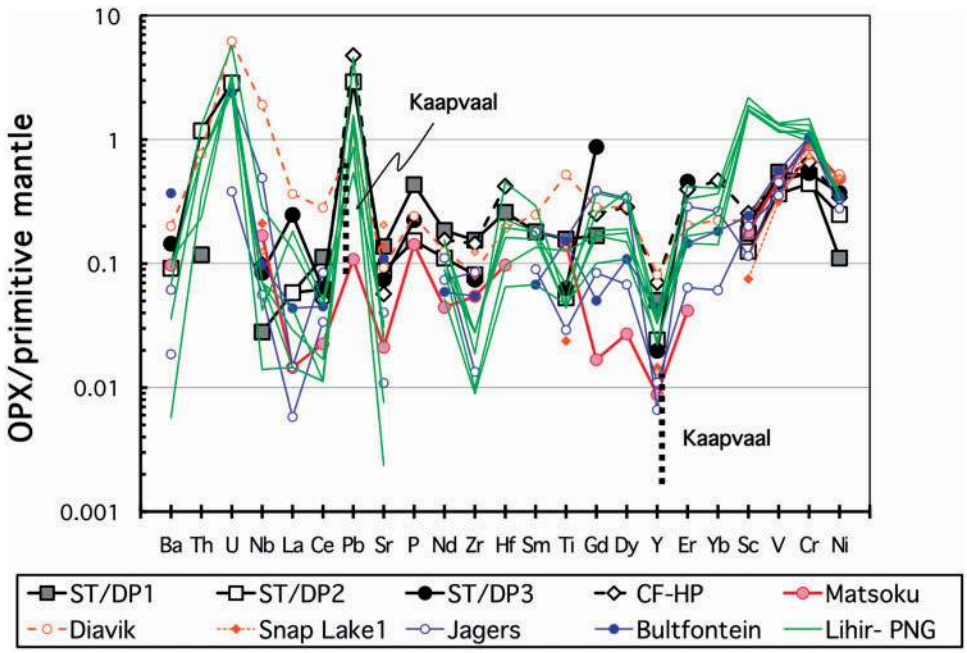

Fig. 9. Trace element abundance patterns for experimental orthopyroxenes measured by laser-ablation ICP-MS, normalized to primitive mantle abundances of Sun & McDonough (1989). Also shown for comparison are data for orthopyroxene in cratonic xenoliths from the following: garnet websterite, Matsoku kimberlite, Lesotho (R. Rapp, this study); garnet peridotites from the Diavik kimberlite, Slave Craton (G. Yaxley, unpublished data), the Snap Lake kimberlite, Slave Craton (Promprated *et al.*, 2004), and the Jagersfontein kimberlite (Grégoire *et al.*, 2003) and the Bultfontein kimberlite (Simon *et al.*, 2007) of the Kaapvaal Craton. Data for orthopyroxene in metasomatized spinel peridotite xenoliths from the sub-arc mantle beneath Papua New Guinea are from Grégoire *et al.* (2001).

laser-ablation data for the experimental melts with those for the coexisting mineral phases (garnet, clinopyroxene, orthopyroxene). In general, the most significant source of error in these estimates is due to incompatible elements that are below the detection limit in the mineral phases, as, with only a few exceptions (Yb in STDP2; Er and Yb in ST/DP3) all the trace elements measured in the melts were above the limits of detection (it should be noted that we do not report maximum D values in Table 5, which could be estimated using the detection limit for certain trace elements in the mineral analyses). The resulting mineral–melt D values prove to be generally consistent with other experimental datasets from the literature, suggesting that mineral–melt equilibrium has been achieved in the experiments. Furthermore, our results indicate that certain trace element characteristics of garnets, clinopyroxenes, and orthopyroxenes in some cratonic samples, both diamond inclusions and xenoliths, provide evidence for metasomatic equilibration with a Mg-rich granitoid melt (sanukitoid), although this signature may have been obscured or overprinted by subsequent metasomatic events.

Garnet–melt D *values*

The two critical factors in analyzing garnet–melt pairs to obtain trace element D values by laser-ablation ICP-MS are the detection limit for elements that are highly incompatible in garnet (e.g. Rb, Ba, Th, U, Pb, Ta, La), and the very low concentrations of some elements because we are using natural, undoped starting materials in our experiments. Nevertheless, the full dataset that we have obtained allows us to calculate garnet–melt D values for a comprehensive group of trace elements (Fig. 10a). Our data show overall consistency with other experimentally determined garnet–melt D values for granitoid melts in equilibrium with eclogite assemblages (Klemme *et al.*, 2002; Xiong, 2006), with several notable exceptions. Except for the HREE (Gd–Yb), Y, Sc, V, Cr and Ni, all measured trace elements are incompatible in garnet. Our D value for Pb is more than an order of magnitude lower than that reported by Klemme *et al.* (2002), which we attribute to the loss of Pb from the melt to the capsule in their experiments. Our D value for Pb is also consistent with that measured for garnet coexisting with hydrous TTG melt (R. Rapp, unpublished data) from a metabasalt dehydration melting experiment carried out at 3·2 GPa, 1075°C, using a graphite-lined Pt capsule (Rapp & Watson, 1995). Our D values for Th and U are likewise an order of magnitude higher than those reported by Klemme *et al.* (2002) and Elkins *et al.* (2008), but these two studies were based on anhydrous experiments conducted at much higher temperatures (≥1400°C); our data for U and Th partitioning, on the other hand, are consistent with the D values for these elements measured in the basalt melting experiment of Rapp & Watson (1995), carried out at at 3·2 GPa and 1075°C. There are also some inconsistencies in the D values for Nb and Ta from the various experimental datasets that will need to be addressed at some point in the future, but given the overall consistency and the comprehensive nature of our dataset, both internally and externally, we argue that the D values we report here should be the preferred values in any trace element-based petrogenetic modelling of melt–rock reaction in the continental lithosphere.

Clinopyroxene–melt D *values*

With few exceptions (Sc, V, Cr, Ni and sometimes Yb), all measured trace elements are incompatible in metasomatic clinopyroxene (Fig. 10b). Again, our data are generally consistent with other experimentally determined clinopyroxene–melt D values for granitoid liquids (e.g. Klemme *et al.*, 2002; Pertermann & Hirschmann, 2002; Elkins *et al.*, 2008). Like the garnet–melt D values, our results for Pb partitioning in clinopyroxene are 4–5 times higher than the only other Cpx–melt D_{Pb} measurement available (Klemme *et al.*, 2002), and we again attribute this discrepancy to preferential loss of Pb from the melt to the platinum capsule in the experiments of Kleeme *et al.* Clinopyroxene in equilibrium with Mg-rich dioritic liquids is capable of fractionating Sc from V ($D_{Sc}/D_V \sim 0{\cdot}12$–$0{\cdot}82$), Zr from Hf ($D_{Zr}/D_{Hf} \sim 0{\cdot}3$–$0{\cdot}5$), and Ce from Pb ($D_{Ce}/D_{Pb} \sim 2{\cdot}2$), driving liquids towards high(er) Sc/V and Zr/Hf ratios, and low(er) Ce/Pb ratios. Because of the low concentrations of Nb, and in particular Ta, in clinopyroxene, we are unable to assess the potential for this phase to fractionate these sister elements from each other during metasomatic reactions involving Mg-rich diorite melts, although it does fractionate La from Nb ($D_{La}/D_{Nb} \sim 1{\cdot}1$–$9{\cdot}6$), contributing to a lowering of La/Nb ratios in the melt.

Orthopyroxene–melt D *values*

Orthopyroxene–melt D values (Fig. 10c) have been determined for a subset of the elements measured (e.g. P, K, Sc, Ti, V, Cr, Ni, Sr, Y, Zr, Nb, La and Ce), because of the low concentrations of these elements in the starting materials (e.g. natural abundance levels), and the high incompatiblity of most trace elements in orthopyroxene. Rough estimates based on sparse data are reported for Hf, Gd, Dy, Er, Yb, Th and Pb. With the exception of V, Cr and Ni, all measured trace elements are incompatible in orthopyroxene in equilibrium with Mg-rich diorite liquids. Our data compare favorably with other experimentally determined D values from Green *et al.* (2000) and McDade *et al.* (2003), with an order of magnitude or less variability between the datasets. Orthopyroxene can fractionate Sc from V (e.g. $D_{Sc}/D_V \sim 0{\cdot}5 \pm 0{\cdot}3$), with Sc being moderately incompatible (average $D \sim 0{\cdot}7$; range ∼0·5–0·9), and V moderately compatible to neutral (average $D \sim 1{\cdot}9$; range ∼1–4). Orthopyroxene produced by melt–rock reaction also fractionates Ni from Cr to a variable extent, showing a preference for Ni, and driving liquids to high $(Cr/Ni)_{PM}$

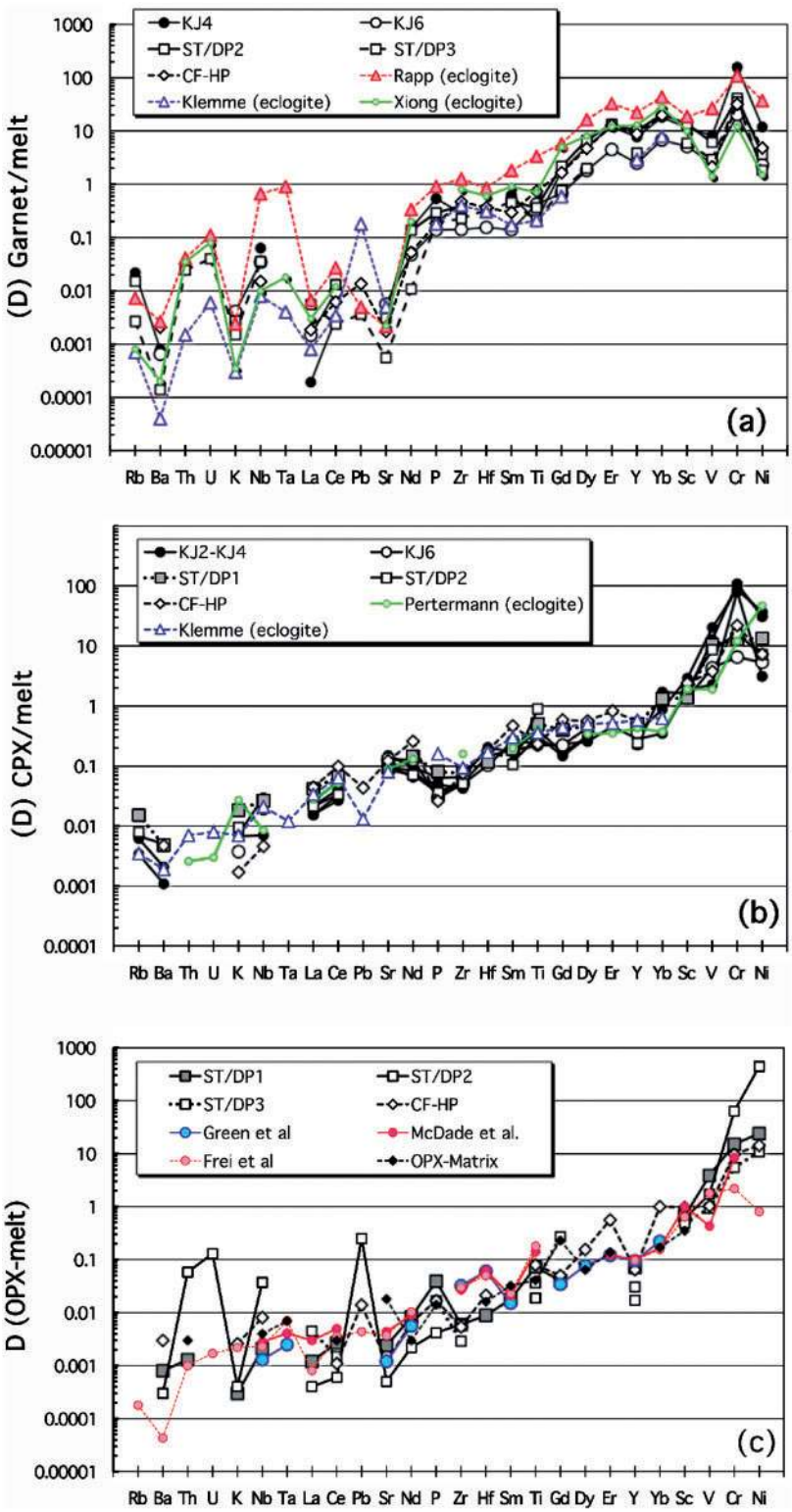

Fig. 10. Experimentally determined trace element mineral–melt D values governing melt–rock reaction in the cratonic lithosphere. (a) Garnet–Mg-rich diorite melt D values from this study compared with published D values for garnet–anhydrous, Fe-free 'tonalitic' melt (Klemme *et al.*, 2002) and garnet–hydrous TTG melt (Xiong, 2006), and unpublished data for garnet–hydrous TTG melts D values from the experiments of Rapp & Watson (1995). (b) Clinopyroxene–Mg-rich diorite melt D values from this study, compared with published D values of Klemme *et al.* (2002) and Pertermann & Hirschmann (2002), both determined under anhydrous conditions. The overall strong correlation between the different datasets, with the exception of lead (Pb), should be noted (see discussion in text). (c) Orthopyroxene–melt D values from this study compared with D values from Green *et al.* (2000) for orthopyroxene–hydrous basaltic melt; McDade *et al.* (2003) for hydrous, high-MgO basaltic melt; Frei *et al.* (2009) for high-Al_2O_3, high-CaO orthopyroxene in equilibrium with anhydrous, Fe-free, NCMAS synthetic melts; and mineral–matrix D values for orthopyroxene–dacite melts from Severs *et al.* (2009).

ratios (see Fig. 4a). The two very different D values for Pb shown in Fig. 10c reflect the problem of Pb loss from the melt in experiments with Au capsules (e.g. STDP2), relative to experiments using Au–Pd capsules (e.g. CF-HP), resulting in a $(D_{Pb})_{Opx\text{-}melt}$ value that is more than an order of magnitude lower in the latter case (preferred value). Despite the considerable scatter in the experimental Opx–melt D values, orthopyroxene appears capable of some fractionation of high field strength elements (HFSE; e.g. Zr, Hf, Nb, Ta, and possibly Ti) from HREE (e.g. Dy, Er, and Yb) (van Westrenen *et al.*, 2001); for example, $D_{Zr}/D_{Yb} < 0{\cdot}2$.

DISCUSSION

The general consensus regarding cratons is that their stability over billions of years of Earth's history can be attributed to the presence of the tectosphere (Jordan, 1978, 1988), and the unique chemical and physical properties of their roots deep in the underlying mantle (for recent reviews see Sleep, 2005; Carlson *et al.*, 2005; Lee & Aeolus, 2006). The stable, 'unsubductable' nature of the granitoid (continental) crust of the cratons is a consequence not only of their inherent buoyancy, but also of their chemical and physical bonding to the underlying SCLM. The tectonic environment that led to cratonization remains a matter of considerable speculation, but syntheses of geological and geophysical data for the most extensively studied craton, the Kaapvaal Craton of southern Africa, suggest that subduction processes played a central role both in the formation of Archean continental crust and in the chemical evolution of early continental lithosphere (Aulbach *et al.*, 2002; James & Fouch, 2002; Schmitz *et al.*, 2004; Bell *et al.*, 2005: Carlson *et al.*, 2005; Simon *et al.*, 2007). [It should be emphasized, in all fairness, that our experimental results only specify some mechanism whereby TTG melts can interact with mantle peridotite, and thus are also compatible with the oceanic plateau-melting model for the 'near-coeval formation' of Archean crust and SCLM proposed by Bedard (2006).]

Geochronological studies of cratonic xenoliths and inclusions in diamonds demonstrate that the timing of SCLM formation (e.g. Pearson *et al.*, 1995; Pearson, 2002; Shirey *et al.*, 2004) occurred over the same broad time span (~3·5–2·9 Ga) as the granitoid magmatism that created the overlying continental crust (Clemens *et al.*, 2006; Moyen *et al.*, 2006). We can use the constraints imposed by our experiments to establish an unequivocal genetic link between granitoid magmatism in the crust and the geochemical evolution of the underlying SCLM, and to evaluate the role that melt–rock reaction may have played in the overall development of cratons in the Archean. This is done by straightforward comparisons between our experimental melts and the minerals of the reaction assemblage, with their natural analogues (Late Archean sanukitoids and eclogite–garnet pyroxenite xenoliths, respectively).

Genetic link between TTG and sanukitoids

Numerous studies have highlighted marked similarities in the trace element characteristics of Archean TTGs and sanukitoids (e.g. Smithies & Champion, 2000; Martin *et al.*, 2005, 2010). The experimental liquids and late Archean sanukitoids both possess the distinctive and unique characteristics of TTG granitoids [e.g. high $(La/Yb)_N$ and Sr/Y coupled with depletions in Y, HREE and HFSE]; these correlations are indicative of a genetic link between the two groups of granitoids, the main difference being the relative 'enrichment' of sanukitoids in 'primitive' (mantle-derived) geochemical characteristics (e.g. high Mg-numbers, high Cr, Ni, and V abundances). Variable enrichment in Cr and Ni reflects the extent of the mantle's direct contribution or 'involvement' in sanukitoid petrogenesis. In Fig. 11a, we compare the PM-normalized trace element abundance patterns of our experimental liquids as a group with those of typical Late Archean sanukitoids from the Superior Province (Stevenson *et al.*, 1999), the Brazilian Craton (Althoff *et al.*, 2000), the Tanzanian Craton (Manya *et al.*, 2007), the Baltic Shield (Lobach-Zhuchenko *et al.*, 2008), and the Kaapvaal Craton (Kleinhanns *et al.*, 2003). The overall shapes of the trace element abundance patterns for the natural rocks are remarkably similar to the experimental melts, with the most prominent features of the experimental liquids (e.g. compared with PM, strong relative depletions in Nb–Ta and Ti, positive Pb anomaly; high K/Nb and V/Cr, and low Ce/Pb ratios) present in the sanukitoid samples as well. These results demonstrate a genetic relationship between sanukitoids and TTG, with parental sanukitoid melts forming by reaction between TTG liquids and mantle peridotite. Our experimental high-Mg diorite (sanukitoid) melts are in equilibrium with olivine-free, garnet clinopyroxenite or garnet websterite phase assemblages. Liquids comparable with HMAs and bajaites in modern subduction zone settings may form by further assimilation of peridotite by these Mg-rich dioritic melts. As of yet, there is no experimental basis for the idea that primary, primitive granitoid liquids, such as high-Mg diorites, sanukitoids, high-magnesian andesites, and bajaites (e.g. Saunders *et al.*, 1987), are the products of partial melting of olivine-bearing metasomatized peridotite, but rather are in equilibrium with pyroxenite mineral assemblage (Rapp *et al.*, 2005).

Comparisons with cratonic xenoliths

As discussed above, the major element compositions of coexisting garnet and clinopyroxene in the peridotite assimilation experiments, where orthopyroxene makes up part of the reaction assemblage, are similar to those of these phases in cratonic xenoliths of the 'intermediate' or

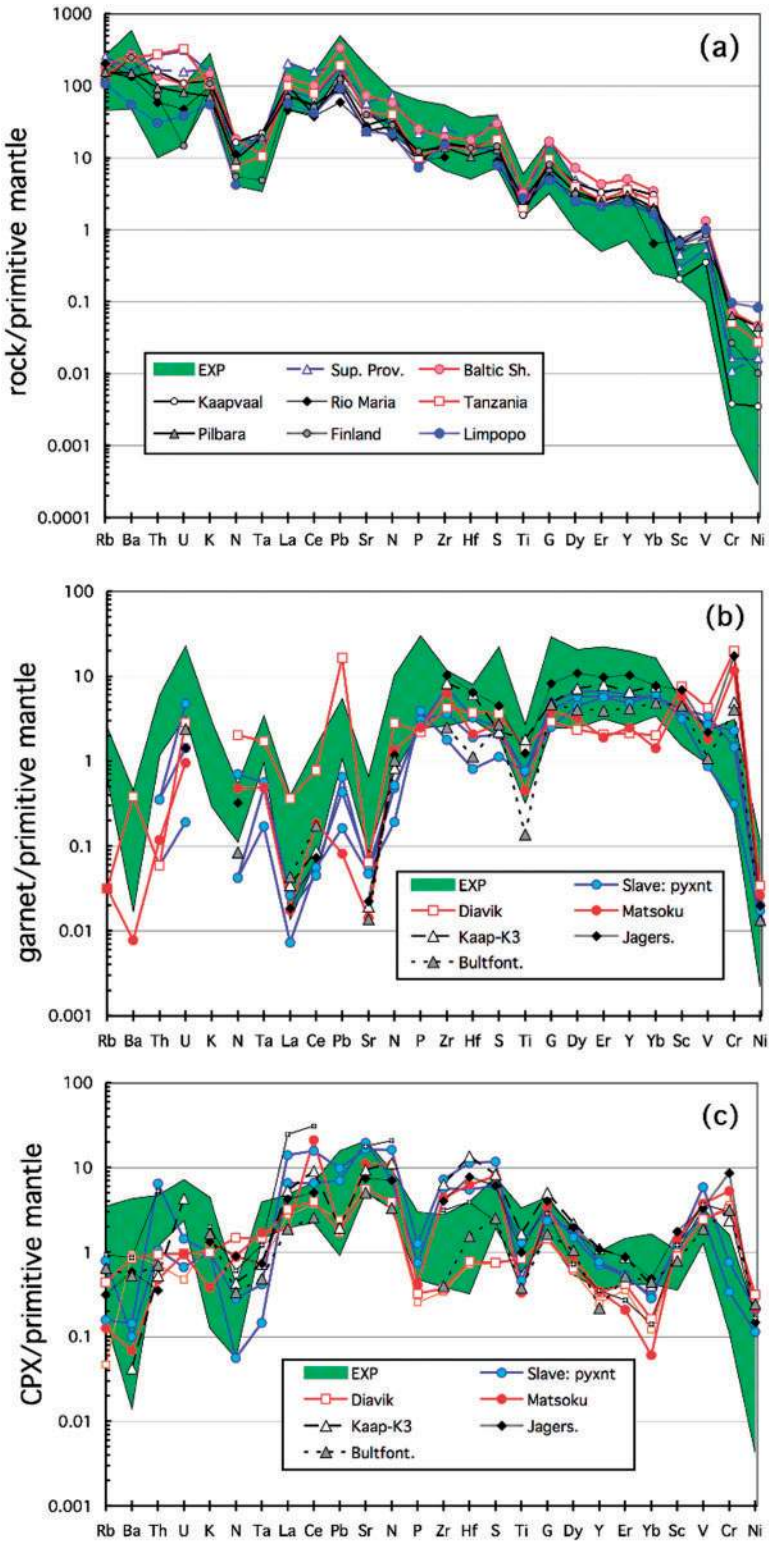

Fig. 11. (a) Primitive mantle normalized trace element abundance patterns of typical Late Archean sanukitoids from various cratons, compared with range of experimental high-Mg diorite (sanukitoid) melts. Data sources: Limpopo Belt, Zimbabwean Craton, Kreissig *et al.* (2000); Barberton Mountain Land, Kaapvaal Craton, Kleinhanns *et al.* (2003); Finland, Fennoscandian Shield, Halla (2005); Baltic Shield, central Karelia, Lobach-Zhuchenko *et al.* (2005, 2008); Pilbara, western Australia, Smithies *et al.* (2004); Superior Province, Canadian Shield, Stevenson *et al.* (1999); Rio Maria granitoids, SE Amazonian Craton, Althoff *et al.* (2000); Tanzanian Craton, Manya *et al.* (2007). (b) Primitive mantle normalized trace element abundance patterns for garnets from cratonic xenoliths compared with the range of patterns observed in experimental garnet samples. Data sources for cratonic samples: Bultfontein and Jagersfontein kimberlites, Kaapvaal Craton, Grégoire *et al.* (2003) and Simon *et al.* (2007); Diavik kimberlite, Slave Craton, Aulbach *et al.* (2007) and G. Yaxley (unpublished data); Matsoku kimberlite, Lesotho, Kaapvaal Craton, R. Rapp (this study). (c) Primitive mantle normalized trace element abundance patterns for clinopyroxenes from cratonic xenoliths compared with the range of patterns observed in experimental clinopyroxene samples. Data sources for cratonic samples are the same as for Fig. 10b.

'websteritic' paragenesis (see Fig. 5, and Sobolev *et al.*, 1999), whereas the major element compositions of garnet and clinopyroxene in the sanukitoid near-liquidus experiments, where orthopyroxene is absent, are similar to those of 'Group B' eclogites of Taylor & Neal (1989), and eclogitic residues of dehydration melting of metabasalt at 2–3 GPa (Rapp & Watson, 1995). Because of the modal predominance of clinopyroxene relative to garnet in the residual phase assemblages in our experiments, we prefer to use the term 'garnet pyroxenite', rather than 'eclogite', although other classification schemes may apply genetic criteria to discriminate these two rock types (e.g. Schulze, 2003; Gonzaga *et al.*, 2010). Thus the near-liquidus experiments (KJ2, KJ3, and KJ4) that we have conducted on the RR-7 starting material indicate that 'parental' sanukitoid liquids would be in equilibrium with a garnet clinopyroxenite mineral assemblage. More Mg-rich HMA or bajaite (see Saunders *et al.*, 1987, for further discussion) liquids would be in equilibrium with garnet websterite or garnet orthopyroxenite mineral assemblages. These differences may be related to a higher proportion of mantle peridotite relative to granitoid liquid in the orthopyroxene-bearing experiments, and the more magnesian nature of the bulk composition, given that all of the experiments were carried out at approximately the same temperature ($1200 \pm 50^{\circ}C$).

Garnet

In Fig. 11b we compare the range of trace element abundances measured in our experimental garnets with the primitive mantle normalized patterns of selected garnets in xenoliths from the Kaapvaal Craton [e.g. from the Matsoku kimberlite in Lesotho (R. Rapp, this study) and the Bultfontein and Jagersfontein kimberlites in South Africa (Grégoire *et al.*, 2004: Simon *et al.*, 2007)], and in garnet pyroxenite and garnet peridotite xenoliths from the Diavik kimberlite in the Slave Craton (Aulbach *et al.*, 2007; G. Yaxley, unpublished data). Although there is considerable variability in the highly incompatible elements on the left-hand side of the diagram, the cratonic samples share a number of the most distinctive features of the experimental garnets, in particular the prominent negative anomalies in Sr and Ti, positive anomalies in U and Pb, and highly fractionated, LREE-depleted REE patterns that are flat from Sm to Yb (see also Fig. 7b). Bearing in mind that the cratonic samples most probably experienced multiple episodes of metamorphism and metasomatism, we consider these similarities to be reasonably strong evidence for a history that includes equilibration with a high-magnesium dioritic (sanukitoid) melt at some point in their evolutionary path.

Clinopyroxene

PM-normalized trace-element abundance patterns for clinopyroxene in mantle xenoliths from the Kaapvaal (Grégoire *et al.*, 2003: Simon *et al.*, 2007) and Slave cratons (Aulbach *et al.*, 2007; G. Yaxley, unpublished data) are shown in Fig. 11c, relative to the range displayed by the experimental Cpx. On this diagram, the natural samples exhibit some of the same distinctive trace element features (relative to primitive mantle abundances) of Cpx in equilibrium with high-Mg diorite (sanukitoid) melts; for example, negative anomalies in Pb (unless phlogopite is present) and Ti, high Cr/Ni and Ce/Pb ratios, and low Pb/Sr and Sc/V ratios, and $Nb/Ta < 1{\cdot}0$, although the fractionation of Nb from Ta in the cratonic samples is not as pronounced as in the experimental samples. Some cratonic samples also show a more pronounced depletion in HREE and enrichment in LREE compared with the experimental samples; these features may be attributable to an SCLM that was initially more depleted than the peridotite starting materials of our experiments, and subsequently subjected to multiple episodes of metasomatism by LREE-enriched fluids. The wide range in trace element abundances of the natural samples may reflect the effects of both multiple metasomatic events and an enhanced susceptibility of clinopyroxene, relative to garnet, to metasomatic alteration; nevertheless, the geochemical characteristics of clinopyroxene that are potentially specific to melt–rock reaction and equilibration with sanukitoid melts [e.g. negative anomalies in Pb and Ti; $(Nb/Ta)_{PM} < 1{\cdot}0$] appear to persist through these events. Corroborating evidence for such an interpretation comes from melt-metasomatized spinel peridotite xenoliths from the sub-arc mantle beneath Papua, New Guinea, whose clinopyroxenes show many of the same distinctive characteristics of the experimental samples, including negative anomalies in Pb and Ti, $(Nb/Ta)_{PM} < 1{\cdot}0$, and high Cr/Ni ratios. Notably, ratios in the PNG xenoliths have $(Sc/V)_{PM} > 1{\cdot}0$, reflecting the absence of garnet in the metasomatic phase assemblage.

Orthopyroxene

Orthopyroxene plays a key role in the melt–rock reactions that are the focus of this study. When formed during assimilation of peridotite by hydrous granitoid liquids (TTG and sanukitoid), orthopyroxene shows a wide compositional range in terms of Mg-number and CaO and Al_2O_3 concentrations, parameters that appear to be related to temperature, melt–rock ratio, and the initial composition of the peridotite being metasomatized. Although the majority of orthopyroxenes in cratonic peridotites, pyroxenites, and inclusions in diamonds have Mg-numbers greater than 0·91, $CaO < 0{\cdot}5$ wt %, and $Al_2O_3 < 1{\cdot}0$ wt % (Fig. 5a and b), the full range of compositions extends beyond this locus to include samples with lower Mg-numbers and higher CaO and Al_2O_3 contents. Orthopyroxene compositions in assimilation experiments between SiO_2-rich melts and peridotite fall within an envelope defined by two different compositional trends in

terms of these components, depending upon whether the initial peridotite is fertile or depleted. For reactions with depleted peridotite, metasomatic orthopyroxene compositions trend towards lower Mg-numbers and higher CaO and Al_2O_3 as the melt:rock ratio increases (Rapp *et al.*, 1999; Fig. 6a and b, this study). For melt–rock reactions involving fertile peridotite, the compositional trend in orthopyroxene is towards higher CaO and Al_2O_3, with only a slight decrease in Mg-number (e.g. Yaxley & Green, 1998). Orthopyroxene diamond inclusions from the Kaapvaal (Aulbach *et al.*, 2002) and Siberian (Sobolev *et al.*, 1997) cratons, and orthopyroxene in garnet pyroxenite xenoliths from Matsoku (Cox *et al.*, 1973; R. Rapp, this study), follow the trend defined by metasomatic orthopyroxene produced in assimilation reactions with depleted peridotite (Rapp *et al.*, 1999; this study). In contrast, peridotite xenoliths from the Slave Craton trend towards the field defined by metasomatic orthopyroxenes produced in melt–rock reactions with fertile peridotite (Yaxley & Green, 1998), particularly with respect to Al_2O_3. Data for orthopyroxenes in metasomatized, suprasubduction zone xenoliths from Papua New Guinea (Grégoire *et al.*, 2001), the Solomon Islands (Berly *et al.*, 2006), and Grenada (Vannucci *et al.*, 2007) in general appear to follow the trend defined by melt–rock reactions with depleted peridotite (as expected, given the subduction setting), with a smaller subset of samples at higher Mg-numbers following the other trend (Figs. 6a and b).

Previous peridotite assimilation experiments at relatively high melt:rock ratios have shown that the stability of metasomatic orthopyroxene is enhanced in depleted peridotite bulk compositions relative to fertile compositions (Johnston & Wyllie, 1989; Rapp *et al.*, 1999). The absence of orthopyroxene in the sanukitoid near-liquidus experiments suggests therefore that Late Archean sanukitoids may have formed by reaction between TTG melts and relatively fertile (or moderately depleted) mantle, at relatively high melt:rock ratios. Based on our experimental results, the extreme enrichment in Mg and related elements (e.g. Ni, Cr, V, etc.) observed in HMAs and bajaites in modern subduction zones requires saturation in orthopyroxene, which is favoured by low melt:rock ratios, strongly depleted mantle peridotite, (possibly) higher temperatures, and in general more protracted melt–rock interaction.

Modification of SCLM by SiO_2-rich melts

Our experimental results demonstrate that granitoid melts with high Mg-numbers, resembling Late Archean sanukitoids or Mg-rich diorites, can form by reaction between initally low Mg-number TTG liquids and mantle peridotite. These mantle-hybridized liquids are virtually identical to sanukitoids from a number of Archean terranes in terms of their major- and trace-element compositions. We have also shown that the trace-element characteristics of minerals in the crystalline component of the melt–rock reaction assemblage (garnet, clinopyroxene, and orthopyroxene) share some of their distinctive features with possible analogue minerals occurring as inclusions in diamonds, or as part of the phase assemblage in xenoliths from the SCLM. Taken together, these results establish a genetic link between Late Archean, generally late- to post-kinematic sanukitoids (Shirey & Hanson, 1984; Smithies & Champion, 2000: Martin *et al.*, 2005), and the latter stages of SCLM evolution, marking the final phase of cratonization. Thus the Neoarchean (3·0–2·5 Ga) Re–Os ages for peridotite xenoliths (Pearson *et al.*, 1995; Irvine *et al.*, 2001) and sulfide inclusions in diamonds (Shirey *et al.*, 2004) from the Kaapvaal Craton coincide with the termination of major crust-building granitoid (sanukitoid) magmatism in the Barberton terrain at ~2·9 Ga.

The cratonic lithosphere's long-term stability is attributable to its low density and high viscosity (Arndt *et al.*, 2009), features that in turn reflect an SCLM that is dry and refractory, composed mineralogically of highly magnesian olivine ($Fo_{92–94}$) with or without orthopyroxene, with a 'melt-depleted', harzburgitic bulk composition (Boyd & Mertzmann, 1987; Boyd, 1989; Lee & Aeolus, 2006). Partial melting experiments on fertile lherzolite bulk compositions suggest that the refractory and chemically depleted nature of the SCLM is a consequence of 30–50% melt extraction, with cratonic peridotites representing the crystalline residue of this melting (Walter, 1998, 1999; Herzberg, 1999, 2004).

Low-temperature, high Mg-number (~93) peridotite xenoliths from the Kaapvaal and Siberian cratons are anomalously rich in SiO_2 and modal orthopyroxene (~30%) (Boyd, 1989; Boyd *et al.*, 1997). One explanation for the high modal orthopyroxene in some cratonic peridotites is by second-stage modal metasomatism, whereby infiltrating SiO_2-rich melts (TTG), generated by partial melting of subducting eclogite, react with the Mg-rich cratonic residues produced in the first stage, forming orthopyroxene at the expense of olivine (Kelemen *et al.*, 1998). In this model, the 'effective melt:rock ratio' (Rapp *et al.*, 1999) is low, and cryptic metasomatism associated with melt–rock reaction imparts a trace element overprint to the peridotite that is reflective of the infiltrating granitoid melts. This two-stage evolution of cratonic lithosphere is consistent with isotopic signatures in xenoliths that document a history of melt–rock metasomatism post-dating the initial depletion events that first isolated the cratonic lithosphere from the convecting mantle (Pearson, 1999). The non-ubiquitous nature of orthopyroxene enrichment in different cratons (e.g. notably weak or absent in the Slave and North Atlantic cratons) is to be expected if melt metasomatism represented a separate, post-depletion stage in the evolution of cratonic lithosphere. Our experimental results are consistent, to a point, with the model of Kelemen *et al.* (1998), in that melt–rock reaction increases

the amount of orthopyroxene in the reaction assemblage relative to olivine, and in the fact that the metasomatized minerals in altered peridotite retain a geochemical record of equilibration with a granitoid melt. Because the melt:rock ratio in our experiments is comparatively high, the reaction residue is pyroxenitic, and a mantle-hybridized melt (sanukitoid or high-Mg diorite liquid) survives the encounter. For melt–rock reaction on a more pervasive scale, where a low melt fraction is percolating through a crystalline matrix, the granitoid melt will have insufficient chemical 'inertia' to transform all of the original olivine to orthopyroxene, and the metasomatic phase assemblage will remain peridotitic. Based upon the existence in the Late Archean rock record of late- to post-tectonic sanukitoid magmatism, orthopyroxene-enriched peridotites, and garnet websterite xenoliths and diamond inclusion parageneses possessing trace element signatures indicative of equilibration with Mg-rich granitoid melts, we conclude that melt–rock reaction played a significant role in the latter stages of craton evolution.

Tectonic setting for crust formation in the Archean

Considerable effort has been devoted to reconstructing the tectonic environment in which continent emergence and growth, SCLM formation, and craton stabilization occurred on the early Earth. Hadean zircons at best attest only to the presence of (some) 'islands' of granitoid crust, not necessarily continents, lacking the necessary roots in the underlying mantle to preserve them, although inclusions of diamonds within these very old zircons (Menneken *et al.*, 2007) suggests that deep recycling of crustal rocks was occurring. And none of these ephemeral oases of very ancient continental crust survive, as far as we know. In this regard then, the question of when and how continental crust became attached, physically and chemically, to lithospheric mantle becomes important, and any evidence for linked evolution of these two domains is particularly significant. Because it is generally accepted that Archean continental crust and the SCLM evolved together (e.g. Pearson *et al.*, 2002; Griffin *et al.*, 2003; Shirey *et al.*, 2004; Bedard, 2006), the preservation of continental crust of early Archean age implies the presence of juvenile SCLM at that time as well.

A number of tectonic models for the formation of subcontinental lithospheric mantle have been proposed, divisible roughly between vertically dominated or horizontally dominated tectonics, plume-related (e.g. Bedard, 2006) or subduction-related (for a variety of subduction-based perspectives see Griffin *et al.*, 2003, 2009; Shirey *et al.*, 2004, 2008; Carlson *et al.*, 2005; Sleep, 2005; Lee & Aeolus, 2006; Arndt *et al.*, 2009). It seems probable that the highly depleted nature of the SCLM is a result of very high degrees of partial melting of an upwelling plume to produce komatiite liquids (Walter, 1998, 1999; Herzberg, 1999). Intra-oceanic collision as a result of convergence of relatively young, hot (possibly thick) Archean oceanic lithosphere (Bickle *et al.*, 1994; Kusky & Polat, 1999; Foley *et al.*, 2003) and fixed oceanic plateaux anchored above mantle plumes may have led to thin-skinned, imbricate thrust-stacking of oceanic lithosphere above or against oceanic plateaux in the early to mid-Archean (e.g. Helmstaedt & Schulze, 1986; de Wit *et al.*, 1992; Nair & Chacko, 2008). Crustal overthickening by the combined effects of horizontal 'flake' tectonics (Hoffman & Ranalli, 1988), flat subduction (Smithies *et al.*, 2004) and delamination of oceanic upper crust (de Wit *et al.*, 1992; Foley *et al.*, 2003), would isolate the hydrous, mafic crustal components of oceanic lithosphere, and continued tectonic thickening would eventually displace this material to depths sufficient to initiate dehydration melting of garnet amphibolite–eclogite to produce low Mg-number TTGs (Rapp *et al.*, 2003). These melts would have experienced little or no interaction with the depleted mantle root of the oceanic plateau (the embryonic SCLM), which would be consistent with the overall dearth of high Mg-number granitoids in the early to mid-Archean. Progressive cooling of the Earth through the Archean would have gradually altered the dynamics of subduction and granitoid magmatism (Martin *et al.*, 2005), either by increasing the depth at which melting of cooler subducted oceanic crust took place (e.g. Martin & Moyen, 2002), or by increasing the angle of subduction (e.g. Smithies & Champion, 2000; Smithies *et al.*, 2004). Both of these conditions would have the effect of introducing a mantle wedge above a subducting slab of oceanic lithosphere, thereby initiating 'modern-style' subduction and arc magmatism.

Based upon geochemical data from well-preserved volcanic sequences in the Pilbara Craton of northwestern Australia, Smithies *et al.* (2007) concluded that there is no compelling evidence for modern-style subduction-related arc magmatism earlier than the Mesoarchean (~3·1 Ga ago), and that 'non-uniformitarian', flat subduction processes may have operated earlier. The ~3·1 Ga age happens to correlate with the intrusion of late- to post-tectonic Mg-rich diorites (sanukitoids) in the Kaapvaal and Zimbabwe cratons (Kreissig *et al.*, 2000; Kleinhanns *et al.*, 2003), and with the peak in Re–Os ages for the Kaapvaal SCLM (Pearson *et al.*, 2002: Shirey *et al.*, 2004; Carlson *et al.*, 2005). A general picture thus emerges that couples continental crust and lithospheric mantle evolution through subduction-related 'arc magmatism', mantle wedge processing and terminal collisional tectonism that culminates in the formation of Archean continental tectosphere (Schmitz *et al.*, 2004).

A general subduction zone setting creates a ready mechanism for the generation and effective transfer of SiO_2-rich melts (TTG) from the subducting slab into the overlying depleted 'wedge' of cratonic lithosphere in the

Late Archean, and also accounts for the silica and incompatible trace element enrichment in cratonic mantle peridotites. Evidence for a possible modern analogue of this scenario is provided by seismic studies of the upper mantle overlying the central Chile–Argentina flat slab, which show anomalously high shear-wave velocities (V_p) and low ratios of compressional- to shear-wave velocities (V_p/V_s). The V_p/V_s ratio has been shown to be highly sensitive to the concentration of orthopyroxene in peridotite (Lee, 2003). The predicted velocities of orthopyroxene-enriched xenoliths from beneath the Kaapvaal Craton and the Colorado Plateau match the observed velocities from the Chile–Argentina upper mantle 'flat slab' transect (Wagner *et al.*, 2008), suggesting a direct relationship between flat slab subduction (in the Archean) and silica enrichment in the continental (cratonic) lithosphere.

SUMMARY

The interdependent physical and chemical processes involved in melt–rock reaction in the SCLM would be expected to be much more complicated than the snapshots provided by 'static' experiments; nevertheless, our results provide equilibrium phase constraints under relevant conditions, to test against the evidence from xenoliths and diamond inclusions, direct samples of the SCLM. The mineral–melt D values that we have determined experimentally can also be used to model more complex processes. Nevertheless, subtle evidence for TTG melt–mantle peridotite interactions at relatively low melt:rock ratios in the Late Archean, by a metasomatic process exemplified by our experimental results, is manifest in the trace element characteristics of single minerals occurring either as inclusions in diamonds or as phases within garnet pyroxenite or orthopyroxene-rich garnet peridotite xenoliths of this age from the SCLM. Late Archean sanukitoid magmatism further suggests that, at least locally, melt:rock ratios were high enough to form plutonic-scale intrusions. Reaction between TTG melts and mantle peridotite thus appears to have occurred over a range of scales, as a crucial stage in craton development.

The geochemical impact and overall intensity of the melt metasomatic event(s) would have been dependent on many variables; our experiments suggest that temperature, the inherent ratio of granitoid melt to peridotite rock, and the initial composition of the infiltrating melt and the ambient mantle all played some role in the extent and outcome of the reaction. The general consequences of these classes of metasomatic reactions between hydrous granitoid melts and peridotitic wall rock can be summarized as follows: (1) 'hybrid' melts retain the characteristic trace element signature of their 'ancestral' TTG melts, but show variable increases in 'primitive' mantle attributes (e.g. Mg-number, Cr, Ni, Sc, V), producing bulk compositions resembling sanukitoid intrusive rocks from the Late Archean, and high-Mg andesites (HMAs) and bajaites in modern arc environments; (2) the reactions produce orthopyroxene at the expense of olivine (which is fully consumed under the conditions of our experiments), producing crystalline residues of garnet websterite and garnet pyroxenite; primary, primitive granitoid melts (sanukitoids, HMAs, bajaites) do not appear to be in equilibrium with olivine-bearing mineral assemblages; (3) metasomatic minerals formed in melt–rock reactions at relatively high melt–rock ratios retain a geochemical signature of their equilibration with granitoid melts; in less 'intense' but perhaps more pervasive metasomatic events (lower temperatures and/or lower melt–rock ratios), these signatures may be more cryptically expressed within the SiO_2- and orthopyroxene-enriched peridotites of the SCLM [e.g. unusually high Ni contents in olivine, as suggested by Kelemen *et al.* (1998)].

ACKNOWLEDGEMENTS

This research was supported by the US National Science Foundation grant number 0044035 to R.P.R., and by a 2005–2006 Visiting Research Fellowship to R.P.R. from the Centre National de la Recherche Scientifique (CNRS) at Université de Blaise Pascal, Clermont-Ferrand. The authors gratefully acknowledge the critical comments of referees James Beard, Kent Condie, and Michel Grégoire. Discussions with Joerg Hermann, Dorrit Jacob, Hugh O'Neill, Anja Rosenthal and Nobu Shimizu helped to improve the manuscript. Assistance with the laser-ablation ICP-MS analyses by Charlotte Allen and Frances Jenner is greatly appreciated.

REFERENCES

Althoff, F., Barbey, F. & Boullier, A.-M. (2000). 2·8–3·0 Ga plutonism and deformation in the SE Amazonian craton: the Archean granitoids of Marajoara (Carajas Mineral Province, Brazil). *Precambrian Research* **104**, 187–206.

Ando, A., Mita, N. & Terashima, S. (1987). 1986 values for fifteen GSJ rock reference samples, 'Igneous rock series'. *Geostandards Newsletter* **11**, 159–166.

Arculus, R. (2006). The andesite model of continental crust origins. *Geochimica et Cosmochimica Acta* **70**, 18 Supplement 1, A20.

Arndt, N. T., Coltice, N., Helmstaedt, H. & Grégoire, M. (2009). Origin of Archean subcontinental lithospheric mantle: some petrological constraints. *Lithos* **109**, 61–71.

Arth, J. G. & Hanson, G. N. (1972). Quartz diorites derived by partial melting of eclogite or amphibolite at mantle depths. *Contributions to Mineralogy and Petrology* **37**, 161–174.

Aulbach, S., Stachel, T., Viljoen, K. S., Brey, G. P. & Harris, J. W. (2002). Eclogitic and websteritic diamond sources beneath the Limpopo Belt—is slab melting the link? *Contributions to Mineralogy and Petrology* **142**, 56–70.

Aulbach, S., Pearson, N. J., O'Reilly, S. Y. & Doyle, B. J. (2007). Origins of xenolithic eclogites and pyroxenites from the central Slave Craton, Canada. *Journal of Petrology* **48**, 1843–1873.

Bedard, J. (2006). A catalytic delamination-driven model for coupled genesis of Archaean crust and sub-continental lithospheric mantle. *Geochimica et Cosmochimica Acta* **70**, 1188–1214.

Bell, D. R., Grégoire, M., Grove, T. L., Chatterjee, N., Carlson, R. W. & Buseck, P. R. (2005). Silica and volatile-element metasomatism of Archean mantle: a xenolith-scale example from the Kaapvaal Craton. *Contributions to Mineralogy and Petrology* **150**, 251–267.

Benoit, M., Aguilon-Robles, A., Calmus, T., Maury, R. C., Bellon, H., Cotton, J., Bourgois, J. & Michaud, F. (2002). Geochemical diversity of Late Miocene volcanism in southern Baja, California, Mexico: implication of mantle and crustal sources during the opening of an asthenospheric window. *Journal of Geology* **110**, 627–648.

Berly, T. J., Hermann, J., Arculus, R. J. & LaPierre, H. (2006). Supra-subduction zone pyroxenites from San Jorge and Santa Isabel (Solomon Islands). *Journal of Petrology* **47**, 1531–1555.

Bickle, M. J., Nisbet, E. G. & Martin, A. (1994). Archean greenstone belts are not oceanic crust. *Journal of Geology* **102**, 121–138.

Bourdon, E., Eissen, J.-P., Gutscher, M.-A., Monzier, M., Samaniego, P., Robin, C., Bollinger, C. & Cotten, J. (2002). Slab melting and slab melt metasomatism in the Northern Andean Volcanic Zone: adakites and high-Mg andesites from Pichincha volcano (Ecuador). *Bull. Soc. Geol. France* **173**(3), 195–206.

Boyd, F. R. (1989). Compositional distinction between oceanic and cratonic lithosphere. *Earth and Planetary Science Letters* **96**, 15–26.

Boyd, F. R. & Mertzmann, S. A. (1987). Composition and structure of the Kaapvaal lithosphere, southern Africa. In: Mysen, B. O. (ed.) *Magmatic Processes: Physicochemical Principles. Geochemical Society Special Publications* **1**, 13–24.

Boyd, F. R., Pokhilenko, N. P., Pearson, D. G., Mertzmann, S. A., Sobolev, N. V. & Finger, L. W. (1997). Composition of the Siberian cratonic mantle: Evidence from Udachnaya peridotite xenoliths. *Contributions to Mineralogy and Petrology* **128**, 228–246.

Calmus, T., Aguillon-Robles, A., Maury, A. C., Bellon, H., Benoit, M., Cotton, J., Bourgois, J. & Michaud, F. (2003). Spatial and temporal evolution of basalts and magnesian andesites ('bajaites') from Baja California, Mexico: the role of slab melts. *Lithos* **66**, 77–105.

Carlson, R. W., Boyd, F. R., Shirey, S. B., Janney, P. E., Grove, T. L., Bowring, S. A., Schmitz, M. D., Bell, D. R., Gurney, J. J., Richardson, S. H., Tredoux, M., Menzies, A. H., Pearson, D. G., Hart, R. J., Wilson, A. H. & Moser, D. (2000). Continental growth, preservation, and modification in southern Africa. *GSA Today* **10**(2), 1–7.

Carlson, R. W., Pearson, D. G. & James, D. E. (2005). Physical, chemical, and chronological characteristics of continental mantle. *Reviews of Geophysics* **43**, 1–24, RG1001.

Carroll, M. J. & Wyllie, P. J. (1989). Experimental phase relations in the system peridotite-tonalite-H_2O at 15 kbar; implications for assimilation and differentiation processes near the crust-mantle boundary. *Journal of Petrology* **30**, 1351–1382.

Clemens, J. C., Yearron, L. M. & Stevens, G. (2006). Barberton (South Africa) TTG magmas: Geochemical and experimental constraints on source-rock petrology, pressure of formation and tectonic setting. *Precambrian Research* **151**, 53–78.

Condie, K. C. (2005). TTGs and adakites: are they both slab melts? *Lithos* **80**, 33–44.

Cox, K. G., Gurney, J. J. & Harte, B. (1973). Xenoliths from the Matsoku Pipe. In: Nixon, P. H. (ed.) *Lesotho Kimberlites*. Maseru: Lesotho National Development Corporation, pp. , pp. 76–100.

de Wit, M. J., Roering, C., Hart, R. J., Armstrong, R. A., de Ronde, C. E. J., Green, R. W. E., Tredoux, M., Peberdy, E. & Hart, R. A. (1992). Formation of an Archaean continent. *Nature* **357**(6379), 553–562.

Elkins, L. J., Gaetani, G. A. & Sims, K. W.W. (2008). Partitioning of U and Th during garnet pyroxenite partial melting: Constraints on the source of alkaline ocean island basalts. *Earth and Planetary Science Letters* **265**, 270–286.

Figueroa, O., Deruelle, B. & Demaiffe, D. (2009). Genesis of adakite-like lavas of Licancabur volcano (Chile–Bolivia, Central Andes). *Comptes Rendus Géoscience* **341**, 310–318.

Foley, S. F., Buhre, S. & Jacob, D. E. (2003). Evolution of the Archean crust by delamination and shallow subduction. *Nature* **421**, 241–252.

Frei, D., Liebscher, A., Franz, G., Wunder, B., Klemme, S. & Blundy, J. (2009). Trace element partitioning between orthopyroxene and anhydrous silicate melt on the lherzolite solidus from 1·1 to 3·2 GPa and 1,230 to 1,535°C in the model system Na_2O–CaO–MgO–Al_2O_3–SiO_2. *Contributions to Mineralogy and Petrology* **157**, 473–490.

Goldich, S. S., Hanson, G. N., Hallford, C. R. & Mudrey, M. G., Jr (1972). Early Precambrian rocks in the Saganaga Lake–Northern Light Lake area, Minnesota–Ontario, Part I: Petrology and structure. In: Doe, B. R. & Smith, D. K. (eds) *Studies in Mineralogy and Precambrian Geology, Geological Society of America, Memoirs* **135**, 151–177.

Gomez-Tuena, A., Langmuir, C. H., Goldstein, S. L., Straub, S. M. & Ortega-Gutierrez, F. (2007). Geochemical evidence for slab melting in the Trans-Mexican volcanic belt. *Journal of Petrology* **48**, 537–562.

Gonzaga, R. C., Lowry, D., Jacob, D. E., LeRoex, A., Schulze, D. & Menzies, M. A. (2010). Eclogites and garnet pyroxenites: similarities and differences. *Journal of Volcanology and Geothermal Research* **190**, 235–2.

Green, T. H., Blundy, J. D., Adam, J. & Yaxley, G. M. (2000). SIMS determination of trace element partition coefficients between garnet, clinopyroxene and hydrous basaltic liquids at 2–7.5 GPa and 1080–1200°C. *Lithos* **53**, 165–187.

Grégoire, M., McInness, B. L. A. & O'Reilly, S. Y. (2001). Hydrous metasomatism of oceanic sub-arc mantle, Lihir, Papua New Guinea Part 2. Trace element characteristics of slab-derived fluids. *Lithos* **59**, 91–108.

Grégoire, M., Bell, D. R. & LeRoux, A. P. (2002). Trace element geochemistry of phlogopite-rich mafic mantle xenoliths: their classification and their relationship to phlogopite-bearing peridotites and kimberlites revisited. *Contributions to Mineralogy and Petrology* **142**, 603–625.

Grégoire, M., Bell, D. R. & Le Roex, A. P. (2003). Garnet lherzolites from the Kaapvaal Craton (South Africa): trace element evidence for a metasomatic hiiostory. *Journal of Petrology* **44**, 629–659.

Grégoire, M., Jego, S., Maury, R. C., Polve, M., Payot, B., Tamayo, R. A., Jr & Yumul, G.P., Jr (2008). Metasomatic interactions between slab-derived melts and depleted mantle: Insights from xenoliths within Monglo adakite (Luzon arc, Philippines). *Lithos* **103**, 415–430.

Griffin, W. L., O'Reilly, S. Y., Abe, N., Aulbach, S., Davies, R. M., Pearson, N. J., Doyle, B. J. & Kivi, K. (2003). The origin and evolution of Archean lithospheric mantle. *Precambrian Res.* **127**, 19–41.

Griffin, W. L., O'Reilly, S. Y., Afonso, J. C. & Begg, G. C. (2009). The composition and evolution of lithospheric mantle: a re-evaluation and its tectonic implications. *Journal of Petrology* **50**, 1185–1204.

Halla, J. (2005). Late Archean high-Mg granitoids (sanukitoids) in the southern Karelian domain, eastern Finland: Pb and Nd isotopic constraints on crust–mantle interactions. *Lithos* **79**, 161–178.

Harrison, T. M. (2009). The Hadean crust: evidence from > 4·0 Ga zircons. *Annual Review of Earth and Planetary Sciences* **37**, 479–505.

Harrison, T. M., Blichert-Toft, J., Muller, W., Albarède, F., Holden, P. & Mojzsis, S. J. (2005). Heterogeneous Hadean hafnium: evidence of continental crust at 4·4 to 4·5 Ga. *Science* **310**, 1947–1950.

Helmstaedt, H. H. & Schulze, D. J. (1986). Southern African kimberlites and their mantle sample: implications for Archean tectonics and lithosphere evolution. In: Ross, J. (ed.) *Kimberlites and Related Rocks. Special Publication of the Geological Society of Australia* **14**, 358–368.

Herzberg, C. (1999). Phase equilibrium constraints on the formation of cratonic mantle. In: Fei, Y., Bertka, C. M. & Mysen, B. O. (eds) *Mantle Petrology, Field Observations and High Pressure Experimentation, a Tribute to Francis R.* (Joe) Boyd: The Geochemical Society, Special Publications **6**, pp. 241–257.

Herzberg, C. (2004). Geodynamic information in peridotite petrology. *Journal of Petrology* **45**, 2507–2530.

Hinton, R. W. (2007). NIST SRM 610, 611 and SRM 612, 613 multi-element glasses: constraints from element abundance ratios measured by microprobe techniques. *Geostandards and Geoanalytical Research* **23**(2), 197–207.

Ila, P. & Frey, F. A. (1999). Trace element analysis of USGS standards AGV2, BCR2, BHVO2, DTS2 and GSP2 by INAA. *Journal of Radioanalytical and Nuclear Chemistry* **244**, 599–602.

Ireland, T. R., Rudnick, R. L. & Spetsius, Z. (1994). Trace elements in diamond inclusions from eclogites reveal link to Archean granites. *Earth and Planetary Science Letters* **128**, 199–213.

Irvine, G. J., Pearson, D. G. & Carlson, R. W. (2001). Lithospheric mantle evolution of the Kaapvaal Craton: A Re–Os isotope study of peridotite xenoliths from Lesotho kimberlites. *Geophysical Research Letters* **28**(13), 2505–2508.

Jacob, D., Jagoutz, E., Lowry, D., Mattey, D. & Kudrjavtseva, G. (1994). Diamondiferous eclogites from Siberia: remnants of Archean oceanic crust. *Geochimica et Cosmochimica Acta* **58**, 5191–5207.

Jacob, D. E., Schmikler, B. & Schulze, D. J. (2003). Trace element geochemistry of coesite-bearing eclogites from the Roberts Victor kimberlite, Kaapvaal craton. *Lithos* **71**, 337–351.

James, D. E. & Fouch, M. J. (2002). Formation and evolution of Archean cratons: insights from southern Africa. In: Fowler, C. M. R., Ebinger, C. J. & Hawkesworth, C. J. (eds) *The Early Earth. Physical, Chemical and Biological Development* Geological Society, London: Special Publications **199**, pp. 1–26.

James, D. E., Fouch, M. J., Vandecar, J. C., van der Lee, S. & Kaapvaal Seismic Group (2001). Tectospheric structure beneath southern Africa. *Geophysical Research Letters* **28**, 2485–2488.

Johnston, A. D. & Wyllie, P. J. (1989). The system tonalite–peridotite–H_2O at 30 kbar, with applications to hybridization in subduction zone magmatism. *Contributions to Mineralogy and Petrology* **102**, 257–264.

Jordan, T. H. (1978). Composition and development of the continental tectosphere. *Nature* **274**, 544–548.

Jordan, T. H. (1988). Structure and formation of the continental tectosphere. *Journal of Petrology, Special Lithosphere Issue* 11–37.

Kelemen, P. D., Hart, S. R. & Bernstein, S. (1998). Silica enrichment in the continental upper mantle via melt/rock reaction. *Earth and Planetary Science Letters* **164**, 387–406.

Kepezhinskas, P., Defant, M. J. & Drummond, M. S. (1995). Na-metasomatism in the island-arc mantle by slab melt–peridotite interaction: evidence from mantle xenoliths in the North Kamchatkan Arc. *Journal of Petrology* **36**, 1505–1527.

Kepezhinskas, P., Defant, M. J. & Drummond, M. S. (1996). Progressive enrichment of island arc mantle by melt–peridotite interaction inferred from Kamchatka xenoliths. *Geochimica et Cosmochimica Acta* **60**, 1217–1229.

Kleinhanns, I. C., Kramers, J. D. & Kamber, B. S. (2003). Importance of water for Archaean granitoid petrology: a comparative study of TTG and potassic granitoids from Barberton Mountain Land, South Africa. *Contributions to Mineralogy and Petrology* **145**, 377–389.

Klemme, S., Blundy, J. D. & Wood, B. J. (2002). Experimental constraints on major and trace element partitioning during partial melting of eclogite. *Geochimica et Cosmochimica Acta* **66**, 3109–3123.

Kreissig, K., Nagler, T. F., Kramers, J. D., van Reenen, D. D. & Smit, C. A. (2000). An isotopic and geochemical study of the northern Kaapvaal Craton and the Southern Marginal Zone of the Limpopo Belt: are they juxtaposed terranes? *Lithos* **50**, 1–25.

Kusky, T. M. & Polat, A. (1999). Growth of granite–greenstone terranes at convergent margins, and stabilization of Archean cratons. *Tectonophysics* **305**, 43–73.

Lee, C.-T. A. (2003). Compositional variation of density and seismic velocities in natural peridotites at STP conditions: Implications for seismic imaging of compositional heterogeneities in the upper mantle. *Journal of Geophysical Research* **108**(B9), 2441.

Lee, A. & Aeolus, C.-T. (2006). Geochemical/Petrologic Constraints on the Origin of Cratonic Mantle. In: Benn, K., Mareschal, J.-C. & Condie, K. C. (eds) *Archean Geodynamics and Environments, Geophysical Monograph Series* **164**, pp. 89–114.

Lobach-Zhuchenko, S. B., Rollinson, H., Chekulaev, V. P., Arestova, N. A., Kovalenko, A. V., Ivanikov, V. V., Guseva, N. S., Sergeev, S. A., Matukov, D. I. & Jarvis, K. E. (2005). The Archean sanukitoid series of the Baltic Shield: geological setting, geochemical characteristics and implications for their origin. *Lithos* **79**, 107–128.

Lobach-Zhuchenko, S. B., Rollinson, H., Chekulaev, V. P., Savatenkov, V. M., Kovalenko, A. V., Martin, H., Guseva, N. S. & Arestova, N. A. (2008). Petrology of a Late Archaean, highly potassic, sanukitoid pluton from the Baltic Shield: insights into Late Archaean mantle metasomatism. *Journal of Petrology* **49**, 393–420.

Manya, S., Maboko, M. A. H. & Nakamura, E. (2007). The geochemistry of high-Mg andesite and associated adakitic rocks in the Musom Mara Greenstone Belt, northern Tanzania: Possible evidence for Neoarchaean ridge subduction? *Precambrian Research* **159**, 241–259.

Martin, H. & Moyen, J.-F. (2002). Secular changes in TTG composition as markers of the progressive cooling of the Earth. *Geology* **30**(4), 319–322.

Martin, H., Peucat, J. J., Sabate, P. & Cunha, J. C. (1997). Crustal evolution in the early Archean of South America: example of the Sete Voltas Massif, Bahia State, Brazil. *Precambrian Research* **82**, 35–62.

Martin, H., Smithies, H., Rapp, R. P., Champion, D. & Moyen, J. F. (2005). An overview of the TTG/adakite/sanukitoid relationship and implications for continental crust genesis and evolution. *Lithos* **79**, 1–24.

Martin, H., Moyen, J.-F. & Rapp, R. P. (2010). The sanukitoid series: magmatism at the Archaean–Proterozoic transition. *Transactions of the Royal Society of Edinburgh* (in press).

McDade, P., Blundy, J. D. & Wood, B. J. (2003). Trace element partitioning between mantle wedge peridotite and hydrous MgO-rich melt. *American Mineralogist* **88**, 1825–1831.

McInnes, B. I. A., Grégoire, M., Binns, R. A., Herzig, P. M. & Hannington, M. D. (2001). Hydrous metasomatism of oceanic sub-arc mantle, Lihir, Papua New Guinea: petrology and geochemistry of fluid-metasomatized mantle wedge xenoliths. *Earth and Planetary Science Letters* **188**, 169–183.

Menneken, M., Nemchin, A. A., Geisler, T., Pidgeon, R. T. & Wilde, S. A. (2007). Hadean diamonds in zircon from Jack Hills, Western Australia. *Nature* **448**, 917–920.

Moyen, J.-F., Stevens, G. & Kisters, A. (2006). Record of mid-Archean subduction from metamorphism in the Barberton terrain, South Africa. *Nature* **442/3**, 559–562.

Nair, R. & Chacko, T. (2008). Role of oceanic plateaus in the initiation of subduction and origin of the continental crust. *Geology* **36**, 583–586.

Nutman, A. P., Bennett, V. C., Friend, C. R. L. & Norman, M. D. (1999). Meta-igneous (non-gneissic) tonalites and quartz-diorites from an extensive ca. 3800 Ma terrain south of the Isua supracrustal belt, southern West Greenland: constraints on early crust formation. *Contributions to Mineralogy and Petrology* **137**, 364–388.

Ota, T., Gladkochub, D. P., Sklyarov, E. V., Mazukabzov, A. M. & Watanabe, T. (2004). *P–T* history of garnet-websterites in the Sharyzhalgai complex, southwestern margin of Siberian craton: evidence for Paleoproterozoic high-pressure metamorphism. *Precambrian Res.* **132**, 327–348.

Pearson, D. G. (1999). The age of continental roots. *Lithos* **48**, 171–194.

Pearson, D. G., Carlson, R. W., Shirey, S. B., Boyd, F. R. & Nixon, P. H. (1995). Stabilization of Archean lithospheric mantle: A Re–Os study of peridotitic xenoliths from the Kaapvaal craton. *Earth and Planetary Science Letters* **134**, 341–357.

Pearson, D. G., Irvine, G. J., Carlson, R. W., Kopylova, M. G. & Ionov, D. A. (2002). The development of lithospheric keels beneath the earliest continents: time constraints using PGE and Re–Os isotope systematics. In: Fowler, C. M. R., Ebinger, C. J. & Hawkesworth, C. J. (eds) *The Early Earth. Physical, Chemical and Biological Development. Geological Society, London, Special Publications* **199**, 65–90.

Pertermann, M. & Hirschmann, M. M. (2002). Trace-element partitioning between vacancy-rich eclogitic clinopyroxene and silicate melt. *American Mineralogist* **87**, 1365–1376.

Petford, N. & Atherton, M. (1996). Na-rich partial melts from newly underplated basaltic crust: the Cordillera Blanca batholith, Peru. *Journal of Petrology* **37**, 1491–1521.

Promprated, P., Taylor, L. A., Anand, M., Floss, C., Sobolev, N. V. & Pokhilenko, N. P. (2004). Multiple-mineral inclusions in diamonds from the Snap Lake/King Lake kimberlite dike, Slave craton, Canada: a trace-element perspective. *Lithos* **77**, 69–81.

Rapp, R. P. & Watson, E. B. (1995). Dehydration melting of metabasalt at 8–32 kbar: Implications for continental growth and crust–mantle recycling. *Journal of Petrology* **36**, 891–931.

Rapp, R. P., Watson, E. B. & Miller, C. F. (1991). Partial melting of amphibolite-eclogite and the origin of Archean trondhjemites and tonalites. *Precambrian Res.* **51**, 1–25.

Rapp, R. P., Shimizu, N., Norman, M. D. & Applegate, G. S. (1999). Reaction between slab-derived melts and peridotite in the mantle wedge: experimental constraints at 3·8 GPa. *Chemical Geology* **160**, 335–356.

Rapp, R. P., Shimizu, N. & Norman, M. D. (2003). Growth of early continental crust by partial melting of eclogite. *Nature* **425**, 605–609.

Rapp, R. P., Laporte, D. & Martin, H. (2005). Adakite induced metasomatism of the mantle wedge: a systematic experimental study at 1·6 GPa. *EOS Transactions, American Geophysical Union* **86**(52), Fall Meeting Supplement, Abstract V31C-0628.

Rogers, G. & Saunders, A. D. (1989). Magnesian andesites from Mexico, Chile and the Aleutian Islands: implications for magmatism associated with ridge–trench collisions. In: Crawford, A. J. (ed.) *Boninites and Related Rocks*. London: Unwin Hyman, pp. , pp. 416–445.

Rogers, G., Saunders, A. D., Terrell, D. J., Verma, S. P. & Marriner, G. F. (1985). Geochemistry of Holocene volcanic rocks associated with ridge subduction in Baja California, Mexico. *Nature* **315**, 389–392.

Saunders, A. D., Rogers, G., Marriner, G. F., Terrell, D. J. & Verma, S. P. (1987). Geochemistry of Cenozoic volcanic rocks, Baja California, Mexico: implications for the petrogenesis of post-subduction magmas. *Journal of Volcanology and Geothermal Research* **32**, 223–245.

Schmitz, M. D., Bowring, S. A., deWit, M. J. & Gartz, V. (2004). Subduction and terrane collision stabilize the western Kaapvaal craton tectosphere 2·9 billion years ago. *Earth and Planetary Science Letters* **222**, 363–376.

Schulze, D. (2003). A classification scheme for mantle-derived garnets in kimberlite: a tool for investigating the mantle and exploring for diamonds. *Lithos* **71**(2–4), 195–213.

Sekine, T. & Wyllie, P. J. (1982). The system granite–peridotite–H_2O at 30 kbar, with applications to hybridization in subduction zone magmatism. *Contrib. Mineral. Petrol.* **81**, 190–202.

Sen, C. & Dunn, T. (1994*a*). Dehydration melting of a basaltic composition amphibolite at 1·5 and 2·0 GPa: implications for the origin of adakites. *Contributions to Mineralogy and Petrology* **117**, 394–409.

Sen, C. & Dunn, T. (1994*b*). Experimental modal metasomatism of a spinel lherzolite and the production of amphibole-bearing peridotite. *Contributions to Mineralogy and Petrology* **119**, 422–432.

Severs, M. J., Beard, J. S., Fedele, L., Hanchar, J. M., Mutchler, S. R. & Bodnar, R. J. (2009). Partitioning behavior of trace elements between dacitic melt and plagioclase, orthopyroxene, and clinopyroxene based on laser ablation ICPMS analysis of silicate melt inclusions. *Geochimica et Cosmochimica Acta* **73**, 2123–2141.

Shirey, S. B. & Hanson, G. N. (1984). Mantle-derived Archaean monzodiorites and trachyandesites. *Nature* **310**, 222–224.

Shirey, S. B., Richardson, S. H. & Harris, J. W. (2004). Integrated models of diamond formation and craton evolution. *Lithos* **77**, 923–944.

Shirey, S. B., Kamber, B. S., Whitehouse, M. J., Mueller, P. A. & Basu, A. R. (2008). A review of the isotopic and trace element evidence for mantle and crustal processes in the Hadean and Archean: Implications for the onset of plate tectonic subduction. In: Condie, K. C. & Pease, V. (eds) *When Did Plate Tectonics Begin? Geological Society of America, Special Papers* **440**, 1–29.

Simon, N. S. C., Carlson, R. W., Pearson, D. G. & Davies, G. R. (2007). The origin and evolution of the Kaapvaal cratonic lithospheric mantle. *Journal of Petrology* **48**(3), 589–625.

Sleep, N. H. (2005). Evolution of the continental lithosphere. *Annual Review of Earth and Planetary Sciences* **33**, 369–93.

Smithies, R. H. (2000). The Archaean tonalite–trondhjemite–granodiorite (TTG) series is not an analogue of Cenozoic adakite. *Earth and Planetary Science Letters* **182**, 115–125.

Smithies, R. H. & Champion, D. C. (2000). The Archaean high-Mg diorite suite: links to tonalite–trondhjemite–granodiorite magmatism and implications for early Archaean crustal growth. *Journal of Petrology* **41**(12), 1653–1671.

Smithies, R. H., Champion, D. C. & Sun, S.-S. (2004). Evidence for early LREE-enriched mantle source regions: diverse magmas from the c. 3·0 Ga Mallina Basin, Pilbara Craton, NW Australia. *Journal of Petrology* **45**, 1515–1537.

Smithies, R. H., Van Kranendonk, M. J. & Champion, D. C. (2007). The Mesoarchean emergence of modern-style subduction. *Gondwana Res.* **11**, 50–68.

Sobolev, N. V., Kaminsky, F. V., Griffin, W. L., Yefimova, E. S., Win, T. T., Ryan, C. G. & Botkunov, A. I. (1997). Mineral inclusions in diamonds from the Sputnik kimberlite pipe, Yakutia. *Lithos* **39**, 135–157.

Sobolev, N. V., Snyder, G. A., Taylor, L. A., Keller, R. A., Yefimova, E. S., Sobolev, V. N. & Shimizu, N. (1998). Extreme chemical diversity in the mantle during eclogite diamond formation: evidence from

35 garnet and 5 pyroxene inclusions in a single diamond. *International Geology Review* **40**, 567–578.

Sobolev, N. V., Sobolev, V. N., Snyder, G. A., Yefimova, E. S. & Taylor, L. A. (1999). Significance of eclogitic and related parageneses of natural diamonds. *International Geology Review* **41**, 129–140.

Stachel, T. & Harris, J. W. (1997). Diamond precipitation and mantle metasomatism—evidence from the trace element chemistry of silicate inclusions in diamonds from Akwatia, Ghana. *Contributions to Mineralogy and Petrology* **129**, 143–154.

Stachel, T., Harris, J. W. & Brey, G. P. (1998*a*). Rare and unusual mineral inclusions in diamonds from Mwadui, Tanzania. *Contributions to Mineralogy and Petrology* **132**, 34–47.

Stachel, T., Viljoen, K. S., Brey, G. & Harris, J. W. (1998*b*). Metasomatic processes in lherzolitic and harzburgitic domains of diamondiferous lithospheric mantle: REE in garnets from xenoliths and inclusions in diamonds. *Earth and Planetary Science Letters* **159**, 1–12.

Stachel, T., Aulbach, S., Brey, G. P., Harris, J. W., Leost, I., Tappert, R. & Viljoen, K. S. (2004). The trace element composition of silicate inclusions in diamonds: a review. *Lithos* **77**, 1–19.

Stern, R. A. & Hanson, G. N. (1991). Archean high-Mg granodiorite: a derivative of light rare-earth enriched monzodiorite of mantle origin. *Journal of Petrology* **32**, 201–238.

Stevenson, R., Henry, P. & Gariepy, C. (1999). Assimilation–fractional crystallization origin of Archean Sanukitoid Suites: Western Superior Province, Canada. *Precambrian Research* **96**, 83–99.

Streckeisen, A. (1976). To each plutonic rock its proper name. Earth-*Science* Reviews **12**, 1–33.

Sun, S. S. & McDonough, W. F. (1989). Chemical and isotopic systematics of oceanic basalts: implications for mantle compositions and processes. In: Saunders, A. D. & Norris, M. J. (eds) *Magmatism in the Ocean Basins. Geological Society, London, Special Publications* **42**, 313–345.

Tatsumi, Y. (2006). High-Mg andesites in the Setouchi Volcanic Belt, southwestern Japan: analogy to Archean magmatism and continental crust formation? *Annual Review of Earth and Planetary Sciences* **34**, 467–499.

Tatsumi, Y., Shukono, H., Sato, K., Shibata, T. & Yoshikawa, M. (2003). The petrology and geochemistry of high-magnesium andesites at the western tip of the Setouchi Volcanic Belt, SW Japan. *Journal of Petrology* **44**, 1561–1578.

Taylor, L. A. & Neal, C. R. (1989). Eclogites with oceanic crustal and mantle signatures from the Bellsbank kimberlite, South Africa. Part I: mineralogy, petrography and whole rock chemistry. *Journal of Geology* **97**(5), 551–567.

Taylor, L. A., Snyder, G. A., Keller, R., Remley, D. A., Anand, M., Wiesli, R., Valley, J. W. & Sobolev, N. V. (2003). Petrogenesis of group A eclogites and websterites: evidence from the Obnazhennaya kimberlite, Yakutia. *Contributions to Mineral and Petrology* **145**, 424–443.

Tsuchiya, N., Suzuki, S., Kimura, J.-I. & Kagami, H. (2005). Evidence for slab melt/mantle reaction: petrogenesis of Early Cretaceous and Eocene high-Mg andesites from the Kitakami Mountains, Japan. *Lithos* **79**, 179–206.

Vannucci, R., Tiepolo, M., Defant, M. J. & Kepezhinskas, P. (2007). The metasomatic record in the shallow peridotite mantle beneath Grenada (Lesser Antilles arc). *Lithos* **99**, 25–44.

van Westrenen, W., Blundy, J. D. & Wood, B. J. (2001). High field strength element/rare earth element fractionation during partial melting in the presence of garnet: Implications for identification of mantle heterogeneities. *Geochemistry, Geophysics, Geosystems* **2**, 2000GC000133.

Wagner, L. S., Anderson, M. L., Jackson, J. M., Beck, S. L. & Zandt, G. (2008). Seismic evidence for orthopyroxene enrichment in the continental lithosphere. *Geology* **36**, 935–938.

Walter, M. J. (1998). Melting of garnet peridotite and the origin of komatiite and depleted lithosphere. *Journal of Petrology* **39**, 29–60.

Walter, M. J. (1999). Melting residues of fertile peridotite and the origin of cratonic lithosphere. In: Fei, Y., Bertka, C. M. & Mysen, B. O. (eds) *Mantle Petrology: Field Observations and High Pressure Experimentation: a Tribute to Francis R.* (Joe) Boyd: The Geochemical Society, Special Publications **6**, pp. 225–239.

Xiong, X.-L. (2006). Trace element evidence for growth of early continental crust by melting of rutile-bearing hydrous eclogite. *Geology* **34**(11), 945–948.

Yaxley, G. M. & Green, D. H. (1998). Reactions between eclogite and peridotite: mantle refertilisation by subduction of oceanic crust. *Schweizerische Mineralogische und Petrographische Mitteilungen* **78**, 243–255.